Electronic Supplementary Information

for

Near Infrared Electroluminescence in Light-emitting Electrochemical Cells from Binuclear Copper(I) Complexes bearing π-extended Benzimidazole and Benzothiazole Ligands

Audrey Fluck,[a,†] Valerio Giuso,[b,†] Chun-Hsi Liu,[c,†] Christophe Gourlaouen,[d] Cristina Cebrián,[e] Federico Polo,[f,g] Hai-Ching Su,[c,*] Abdelaziz Jouaiti,[a,*] and Matteo Mauro,[b,e,*]

[a] *Laboratoire de Synthèse et Fonctions des Architectures Moléculaires, UMR7140 Chimie de la Matière Complexe, Université de Strasbourg & CNRS, 4 rue Blaise Pascal 67000 Strasbourg (France). E-mail: jouaiti@unistra.fr*

[b] *Université de Strasbourg & CNRS, Institut de Physique et Chimie des Matériaux de Strasbourg UMR 7504, F-67034 Strasbourg, France*

[c] *Institute of Lighting and Energy Photonics, National Yang Ming Chiao Tung University, Tainan 71150, Taiwan. E-mail: haichingsu@nycu.edu.tw*

[d] *Laboratoire de Modélisation et Simulations Moléculaires, UMR 7140 Chimie de la Matière Complexe, Institut Le Bel, F-67081 Strasbourg, France*

[e] *Department of Chemical Sciences, University of Padova, Via Marzolo 1, 35121 Padova, Italy. E-mail: matteo.mauro@unipd.it*

[f] *Department of Molecular Sciences and Nanosystems, Ca' Foscari University of Venice, Via Torino 155, 30172 Venezia (Italy)*

[g] *European Centre for Living Technology (ECLT), Ca' Bottacin, 30124, Venice, Italy*

† These authors equally contributed to the work.

Experimental section

General synthetic considerations

^{1}H, $^{13}C\{^{1}H\}$ and $^{31}P\{^{1}H\}$ NMR spectra were recorded at 298 K on either a Bruker AV300 or AV500 spectrometer in deuterated solvents and the residual solvent peak was used as the internal reference. All the chemical shifts (δ) are reported in ppm. High-resolution electrospray mass spectrometry (HR-ESI-MS) was performed by the Service Spectrométrie de Masse of the Fédération de Chimie "Le Bel" UAR2042 of the University of Strasbourg and spectra were recorded on a MicroToF Bruker equipped with an electrospray ionization source.

1*H*-Benzimidazole-2-carboxaldehyde, $[Cu(CH_3CN)_4]PF_6$, dithiooxamide and oxy-di-2,1-phenylene)bis(diphenylphosphine) (DPEPhos) are commercially available and were used as received from Aldrich Chemicals, Acros or BLDPharm. Solvents and other commonly available reagents were purchased and used without further purification.

The synthesis of 1-phenyl-1*H*-benzo[*d*]imidazole-2-carbaldehyde **3**, was carried out in two steps following previously reported procedures[1] and the chemical analyses and reaction yields agrees well with the reported data.

Synthetic procedures

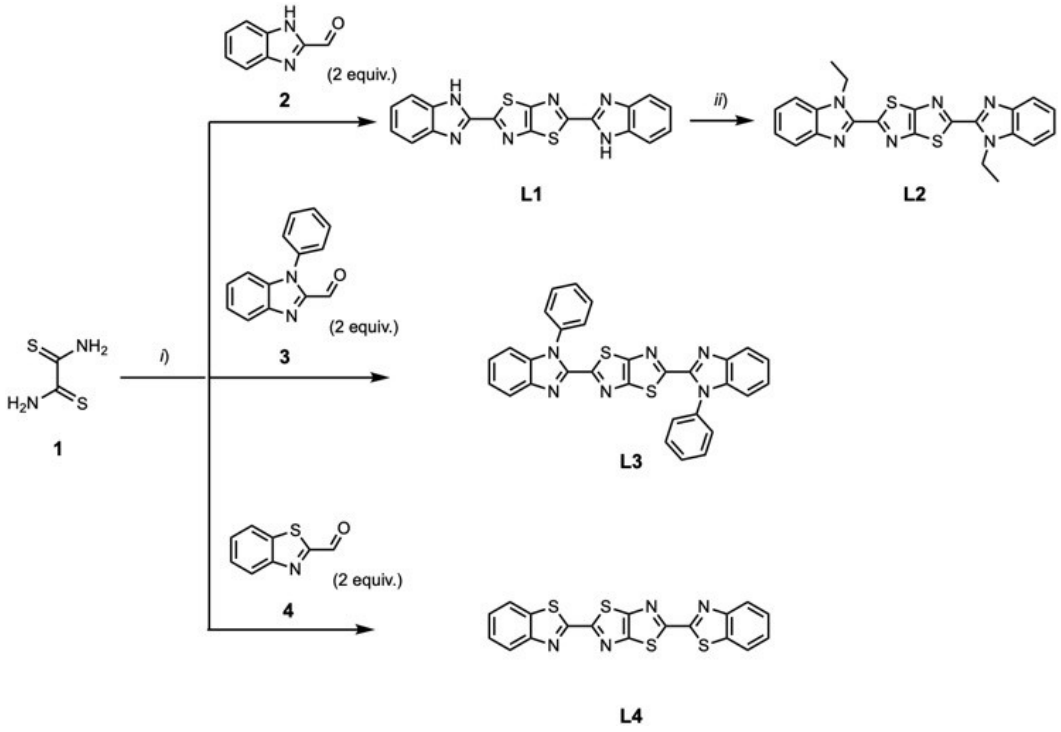

Scheme S1. Synthetic pathway employed for the synthesis of the ligands **L1-L4**. Conditions: *i*) DMF, reflux, 24 hours; *ii*) ethyl bromide, K_2CO_3, DMF, 90 °C, 16 hours.

2,5-*bis*(1H-benzo[*d*]imidazol-2-yl)thiazolo[5,4-*d*]thiazole (**L1**).

1H-benzo[d]imidazole-2-carbaldehyde (1.0 g, 6.84 mmol) was suspended in DMF (20 mL) and the mixture was degassed with Ar. Dithiooxamide (411 mg, 3.42 mmol) was added and the mixture was refluxed under Ar for 24 hours. After cooling down the mixture at room temperature, the formed precipitate was filtered off, washed with MeOH and dried to give the expected product as a light brown solid. (509 mg, yield 40%). The $^{13}C\{^{1}H\}$ NMR of this compound could not be recorded due to its low solubility. ^{1}H NMR (300 MHz, DMSO-d_6) δ (ppm): 13.73 (br s, 2H), 7.75 (br s,2H), 7.60 (br s, 2H), 7.33 (br s, 4H). HR-MS (ESI): m/z $[M + H]^+$ calcd for $C_{18}H_{11}N_6S_2$ $[M + H]^+$ 375.0481, found 375.0496. Elemental analysis: Calculed for $C_{18}H_{10}N_6S_2$. 3 H_2O : C, 50.46; H, 3.76; N, 19.61. Found : C, 50.08 ; H, 2.43, N, 19.20

2,5-*bis*(1-ethyl-1H-benzo[*d*]imidazol-2-yl)thiazolo[5,4-*d*]thiazole (**L2**).

2,5-*bis*(1*H*-benzo[*d*]imidazol-2-yl)thiazolo[5,4-*d*]thiazole (200 mg, 0.53 mmol) was suspended in DMF (5 mL) and the mixture was degassed with Ar. K_2CO_3 (360 mg, 2.62 mmol) and then iodoethane (125 µL, 1.56 mmol) were added and the mixture that was heated at 90°C under Ar for 48 hours. After cooling down at room temperature, the formed precipitate was filtered off, washed with water then MeOH and dried to give the expected product as a yellow powder (179 mg, 78% yield). The $^{13}C\{^{1}H\}$ NMR of this compound could not be recorded due to its low solubility. ^{1}H NMR (500 MHz, $CDCl_3$) δ (ppm): 7.87 (d, J = 7.7 Hz, 2H), 7.50 (d, J = 8.0 Hz, 2H), 7.44–7.33 (m, 4H), 4.96 (q, J = 7.1 Hz, 4H), 1.58 (t, J = 7.3 Hz, 6H). HR-MS (ESI): m/z $[M + H]^+$ calcd for $C_{22}H_{19}N_6S_2$ $[M + H]^+$ 431.1107, found 431.1086. Elemental analysis: Calculed for $C_{22}H_{18}N_6S_2$. H_2O : C, 58.91; H, 4.49; N, 18.74. Found : C, 58.51 ; H, 3.94 ; N, 18.39.

2,5-*bis*(1-phenyl-1*H*-benzo[*d*]imidazol-2-yl)thiazolo[5,4-*d*]thiazole (**L3**).

1-phenyl-1*H*-benzo[*d*]imidazole-2-carbaldehyde (377 mg, 1.7 mmol) was suspended in DMF (5 mL) and the mixture was degassed with Ar. Dithiooxamide (102 mg, 0.85 mmol) was added and the mixture was refluxed under Ar for 24 hours. After cooling down the mixture at room temperature, the formed precipitate was filtered off, washed with MeOH and dried to give the expected product as a yellow solid (216 mg, 48% yield). ^{1}H NMR (500 MHz, $CDCl_3$) δ (ppm): 7.90 (dt, J = 8.2, 0.9 Hz, 2H), 7.60–7.58 (m, 6H), 7.47–7.42 (m, 4H), 7.38 (ddd, J = 8.1, 7.1, 1.2 Hz, 2H), 7.32 (ddd, J = 8.2, 7.1, 1.2 Hz, 2H), 7.17 (dt, J = 8.0, 1.0 Hz, 2H). $^{13}C\{^{1}H\}$ NMR (126 MHz, $CDCl_3$) δ (ppm): 160.1, 152.8, 145.1, 142.8, 138.3, 136.2, 129.8, 129.5, 128.1, 125.2, 124.1, 120.6, 111.2. HR-MS (ESI): m/z $[M + H]^+$ calcd for $C_{30}H_{19}N_6S_2$ $[M + H]^+$

527.1107, found 527.1087. Elemental analysis: Calculed for $C_{30}H_{18}N_6S_2$: C, 68.42; H, 3.45; N, 15.96. Found: C, 68.24; H, 3.42; N, 15.80. Single crystals suitable for RX diffraction analysis were obtained from $CDCl_3$ (CCDC 2402732)

2,5-bis(benzo[d]thiazol-2-yl)thiazolo[5,4-d]thiazole (**L4**).

Benzo[d]thiazole-2-carbaldehyde (1.0 g, 6.12 mmol) was suspended in DMF (20 mL) and the mixture was degassed with Ar. Dithiooxamide (0.367 g, 3.06 mmol) was added and the mixture was refluxed under Ar for 24 hours. After cooling down to room temperature, the formed precipitate was filtered off, washed with MeOH and dried to give the expected product as a light brown solid (0.700 g, yield 56%). Due to its low solubility the ^{1}H NMR and ^{13}C{^{1}H} NMR of this compound could not be performed, and the product was used as obtained for the following step. Elemental analysis: Calculed for $C_{18}H_8N_4S_4$: C, 52.92; H, 1.97; N, 13.71. Found: C, 52.94; H, 1.96; 13.58.

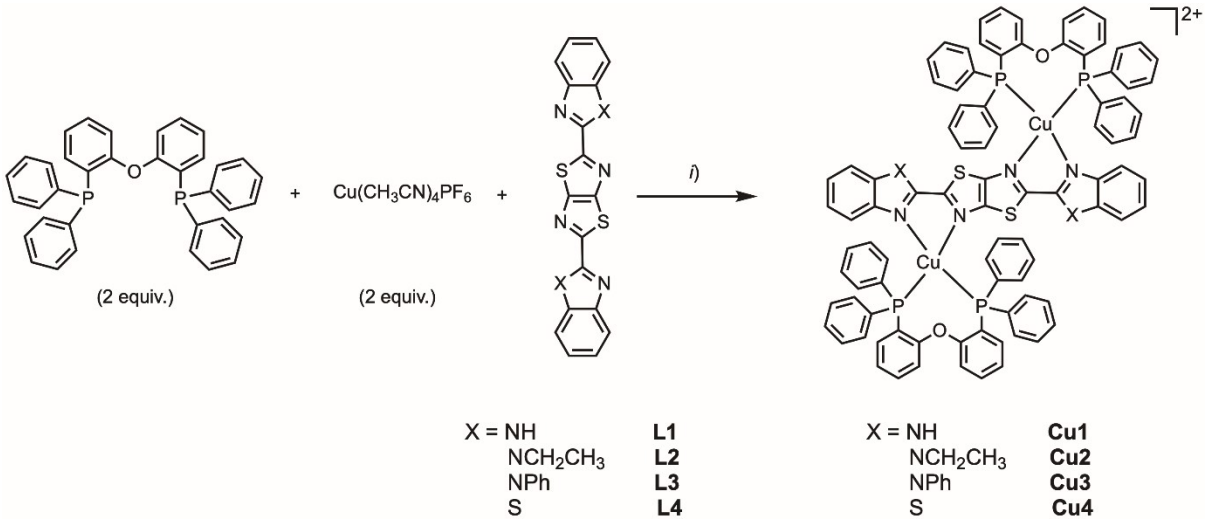

Scheme S2. Synthetic pathway employed for the synthesis of dinuclear compounds **Cu1, Cu2** and **Cu3** prepared as PF_6^- salt. Conditions: *i*) $[Cu(CH_3CN)_4]PF_6$ (2 equiv.), DPEPhos (2 equiv.) and the corresponding ligand **L1**–**L4** (2 equiv.), CH_2Cl_2, room temperature

Synthesis of complex $[Cu_2(DPEPhos)_2(L1)](PF_6)_2$ (**Cu1**).

Under a stream of argon, DPEPhos (188 mg, 0.35 mmol) was dissolved in CH_2Cl_2 (28 mL), $[Cu(CH_3CN)_4]PF_6$ (129 mg, 0.35 mmol) was added and the mixture was stirred under Ar for 5 min. 2,5-bis(1*H*-benzo[*d*]imidazol-2-yl)thiazolo[5,4-*d*]thiazole (**L1**) (65 mg, 0.17 mmol) was added and the mixture was stirred under argon at room temperature for 5 days, until it turned into a clear reddish solution. The mixture was concentrated to almost dryness, Et_2O was added and the red-orange precipitate was washed three times with Et_2O and dried to give the expected product as a dark orange solid (287 mg, 90% yield). ^{1}H NMR (300 MHz, CD_2Cl_2) δ (ppm): 11.42 (s, 2H), 7.83 (d, J = 8.1 Hz, 2H), 7.48–7.29 (m, 12H), 7.28–7.19 (m, 6H), 7.18–7.06 (m,

28H), 7.05–6.94 (m, 12H), 6.86–6.77 (m, 4H). ^{31}P NMR (121.5 MHz, CD_2Cl_2) δ (ppm): –12.50, –143.53 (hept, J = 713.7 Hz). HR-MS (ESI): m/z $[M + H]^+$ calcd for $C_{90}H_{65}Cu_2N_6O_2P_4S_2$ $[M + H]^+$ 1575.2147, found 1575.2133. Crystals suitable for RX diffraction were obtained by vapour diffusion of Et_2O into an acetone solution of the complex (CCDC 2402730).

Synthesis of complex $[Cu_2(DPEPhos)_2(L2)](PF_6)_2$ (**Cu2**).

Under a stream of argon, DPEPhos (150 mg, 0.28 mmol) was dissolved in CH_2Cl_2 (23 mL), $[Cu(CH_3CN)_4]PF_6$ (104 mg, 0.28 mmol) was added and the mixture was stirred under Ar for 5 min. 2,5-*bis*(1-ethyl-1*H*-benzo[*d*]imidazol-2-yl)thiazolo[5,4-*d*]thiazole (**L2**) (60 mg, 0.14 mmol) was added. The mixture turned red and it was stirred at room temperature under Ar for 4 hours. The mixture was concentrated to almost dryness, Et_2O was added and the orange precipitate was washed three times with Et_2O and dried to give the expected product as a bright orange solid (251 mg, 93% yield). ^{1}H NMR (300 MHz, CD_2Cl_2) δ (ppm): 7.67 (dd, J = 10.0, 8.4 Hz, 4H), 7.60–7.52 (m, 2H), 7.47–7.31 (m, 18H), 7.29–7.21 (m, 8H), 7.18–7.09 (m, 12H), 7.03–6.96 (m, 4H), 6.91 (t, J = 7.5 Hz, 8H), 6.83–6.73 (m, 8H), 4.40 (q, J = 7.2 Hz, 4H), 1.50 (t, J = 7.3 Hz, 6H). ^{31}P NMR (121.5 MHz, CD_2Cl_2) δ (ppm) = –12.45, –143.79 (hept, J = 713.7 Hz). HR-MS (ESI): m/z $[M + H]^+$ calcd for $C_{94}H_{74}Cu_2F_6N_6O_2P_5S_2$ $[M + H]^+$ 1777.2493, found 1777.2490. Crystals suitable for RX diffraction were obtained by vapour diffusion of Et_2O into an acetone solution of the complex (CCDC 2402731).

Synthesis of complex $[Cu_2(DPEPhos)_2(L3)](PF_6)_2$ (**Cu3**).

Under a stream of argon, DPEPhos (123 mg, 0.23 mmol) was dissolved in CH_2Cl_2 (18 mL), $[Cu(CH_3CN)_4]PF_6$ (85 mg, 0.23 mmol) was added and the mixture was stirred under Ar for 5 min. 2,5-*bis*(1-phenyl-1*H*-benzo[*d*]imidazol-2-yl)thiazolo[5,4-*d*]thiazole (**L3**) (60 mg, 0.11 mmol) was added. The mixture turned red and it was stirred at room temperature under Ar for 4 hours. The mixture was concentrated to almost dryness, Et_2O was added and the orange precipitate was washed three times with Et_2O 3 and dried to give the expected product as a bright orange solid (215 mg, 97% yield). ^{1}H NMR (300 MHz, CD_2Cl_2) δ: 7.99–7.81 (m, 6H), 7.58 (d, J = 7.9 Hz, 2H), 7.47–7.18 (m, 36H), 7.16–7.06 (m, 6H), 7.03–6.90 (m, 12H), 6.88–6.72 (m, 12H). ^{31}P NMR (121 MHz, CD_2Cl_2) δ: –12.07, –144.49 (p, J = 708 Hz). HR-MS (ESI): m/z $[M + H]^+$ calcd for $C_{102}H_{74}Cu_2F_6N_6O_2P_5S_2$ $[M + H]^+$ 1873.2493, found 1873.2437. Crystals suitable for RX diffraction were obtained by vapour diffusion of Et_2O into an acetone solution of the complex (CCDC 2402732).

Synthesis of complex $[Cu_2(DPEPhos)_2(L4)](PF_6)_2$ (**Cu4**).

Under a stream of argon, DPEPhos (0.263 g, 0.48 mmol) was dissolved in CH_2Cl_2 (20 mL), $[Cu(CH_3CN)_4]PF_6$ (0.181 g, 0.48 mmol) was added and the mixture was stirred under Ar for 5 min. 2,5-*bis*(benzo[*d*]thiazol-2-yl)thiazolo[5,4-*d*]thiazole (**L4**) (0.1 g, 0.24 mmol) was added and the mixture was stirred at room temperature under Ar for 3 days and until it turned into a clear reddish solution. The mixture was concentrated to almost dryness, then Et_2O was added and the red-orange precipitate was washed three times with Et_2O and dried to give the expected product as a red solid (0.380 mg, 98% yield). ^{1}H NMR (500 MHz, CD_2Cl_2) δ (ppm): 8.12 (d, J = 10 Hz, 2H), 7.86 (d, J = 10 Hz, 2H), 7.61 (t, J = 10 Hz, 2H), 7.49 (t, J = 10 Hz, 2H), 7.43 – 6.86 (br m, 56H). ^{31}P{^{1}H} NMR (121.5 MHz, CD_2Cl_2) δ (ppm): –12.54, –143.57 (hept, J = 713.7 Hz). HR-MS (ESI): m/z $[M + H]^+$ calcd for $C_{54}H_{36}CuN_4OP_2S_4$ $[M + H]^+$ 1009.0538, found 1009.0529. Crystals suitable for RX diffraction were obtained by vapour diffusion of Et_2O into a $CHCl_3$ solution of the complex (CCDC 2412038).

NMR Spectra

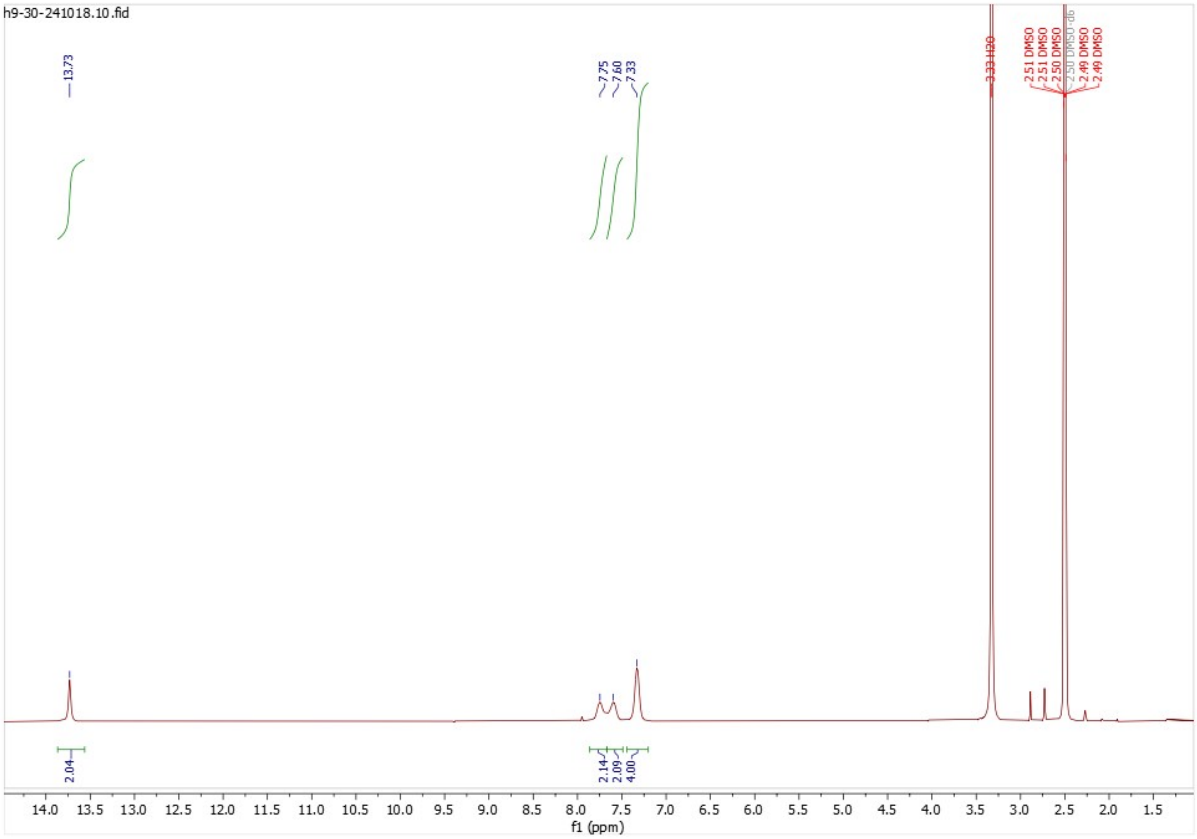

Figure S1. ^{1}H NMR (300 MHz, DMSO-d_6, 298 K) spectrum recorded for compound **L1**.

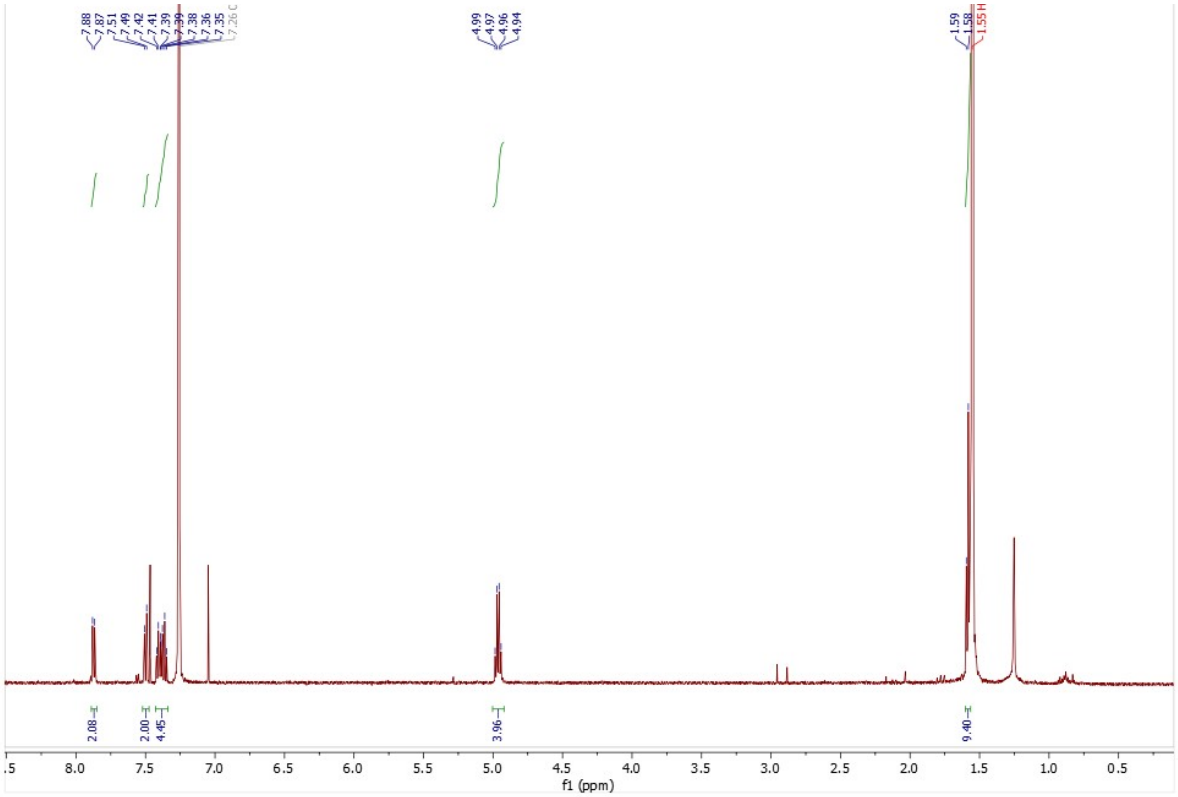

Figure S2. ^{1}H NMR (300 MHz, $CDCl_3$, 298 K) spectrum recorded for compound **L2**.

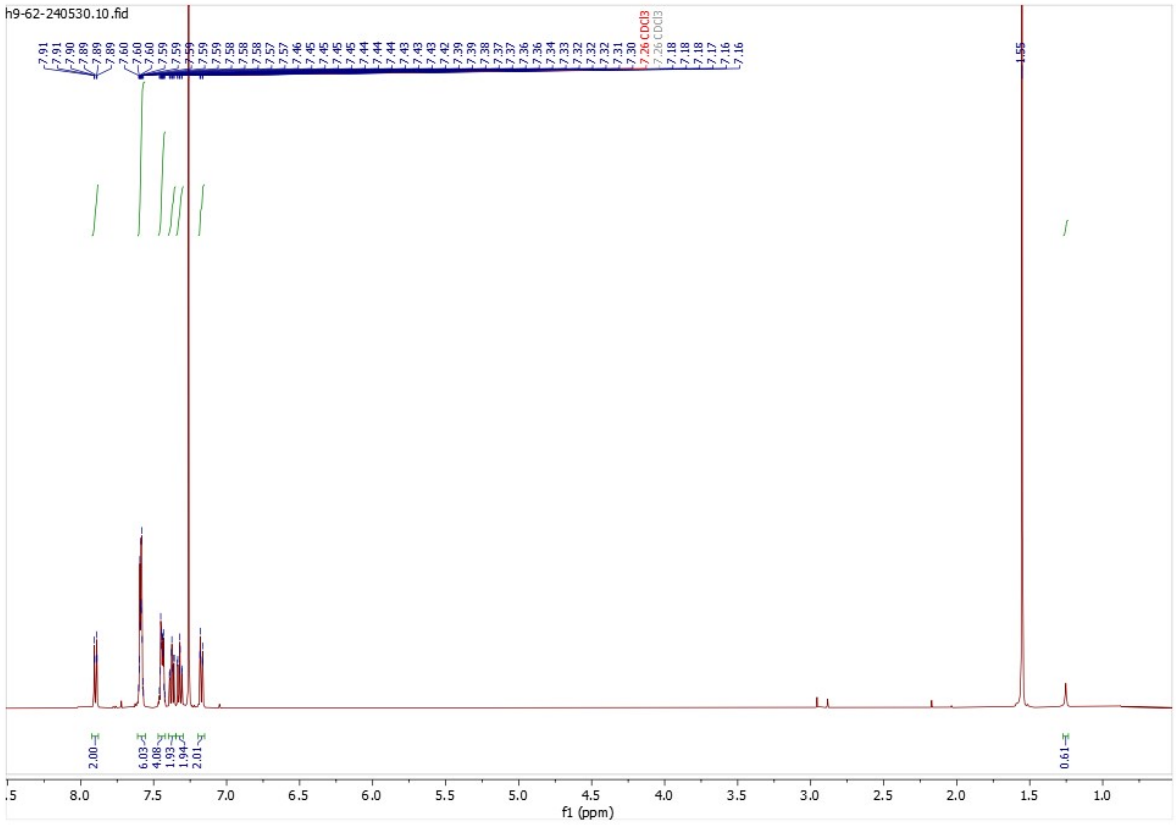

Figure S3. ^{1}H NMR (300 MHz, $CDCl_3$, 298 K) spectrum recorded for compound **L3**.

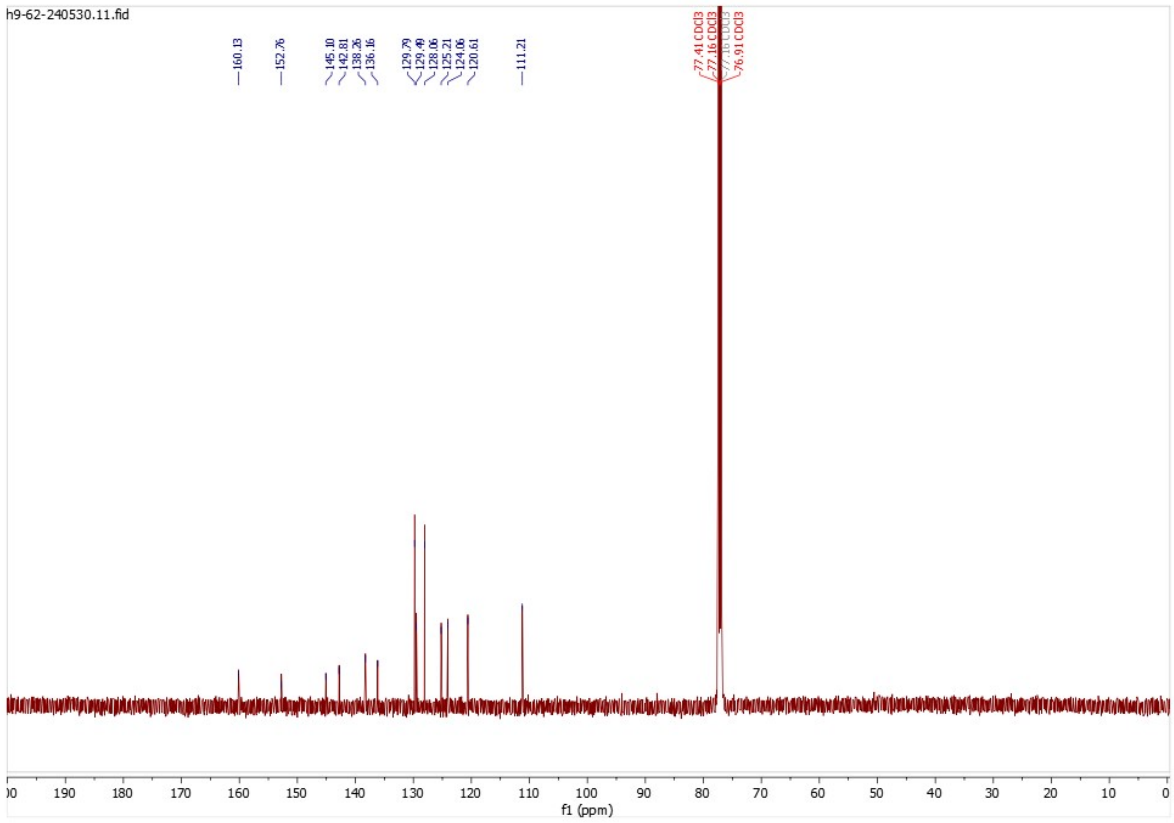

Figure S4. $^{13}C\{^{1}H\}$ NMR (125 MHz, $CDCl_3$, 298 K) spectrum recorded for compound **L3**.

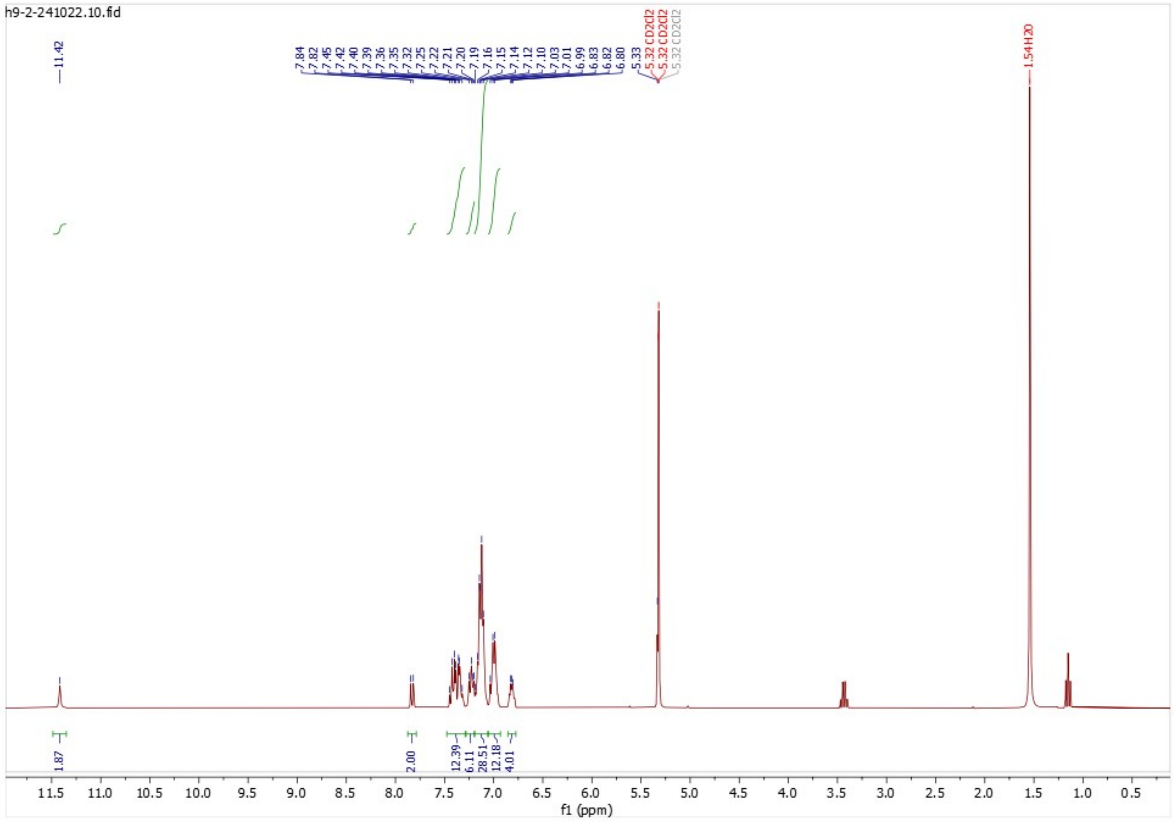

Figure S5. ^{1}H NMR (300 MHz, CD_2Cl_2, 298 K) spectrum recorded for compound **Cu1.**

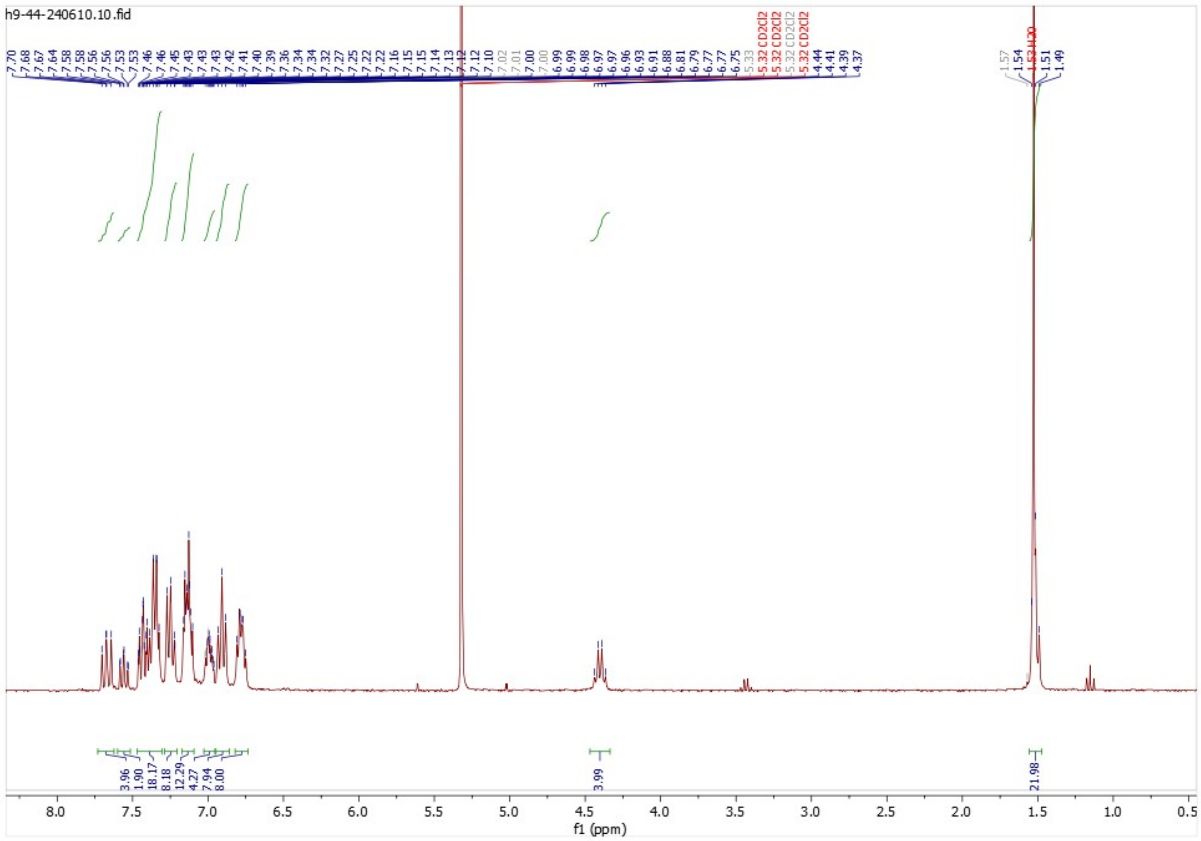

Figure S6. ^{1}H NMR (300 MHz, CD_2Cl_2, 298 K) spectrum recorded for compound **Cu2.**

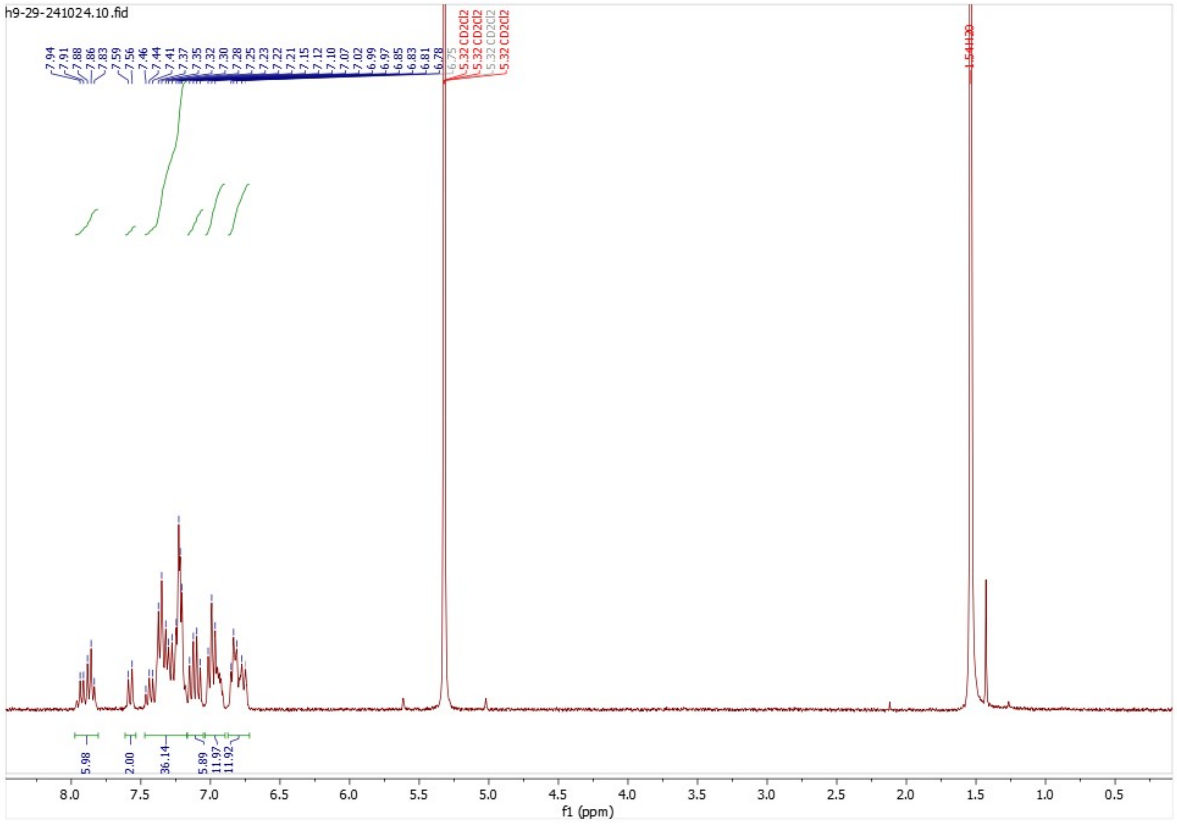

Figure S7. ^{1}H NMR (300 MHz, CD_2Cl_2, 298 K) spectrum recorded for compound **Cu3.**

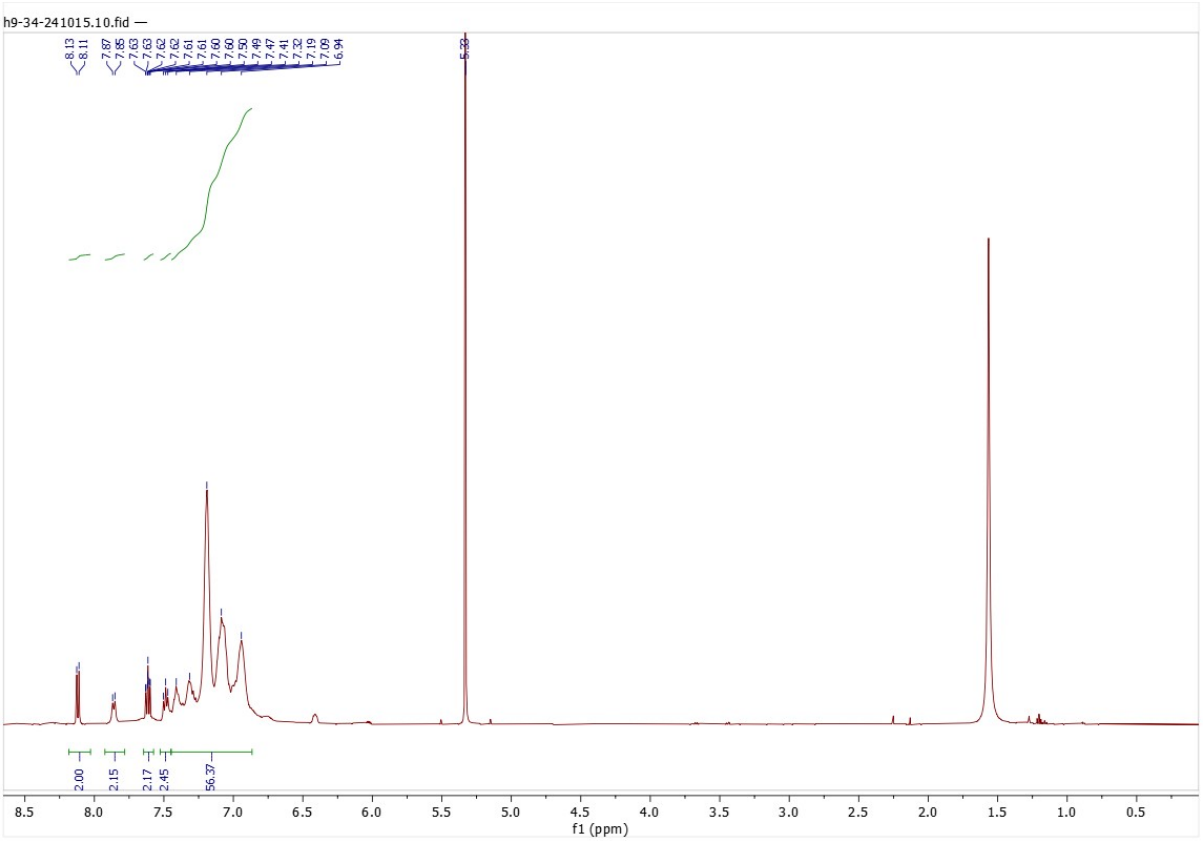

Figure S8. ^{1}H NMR (500 MHz, CD_2Cl_2, 298 K) spectrum recorded for compound **Cu4**.

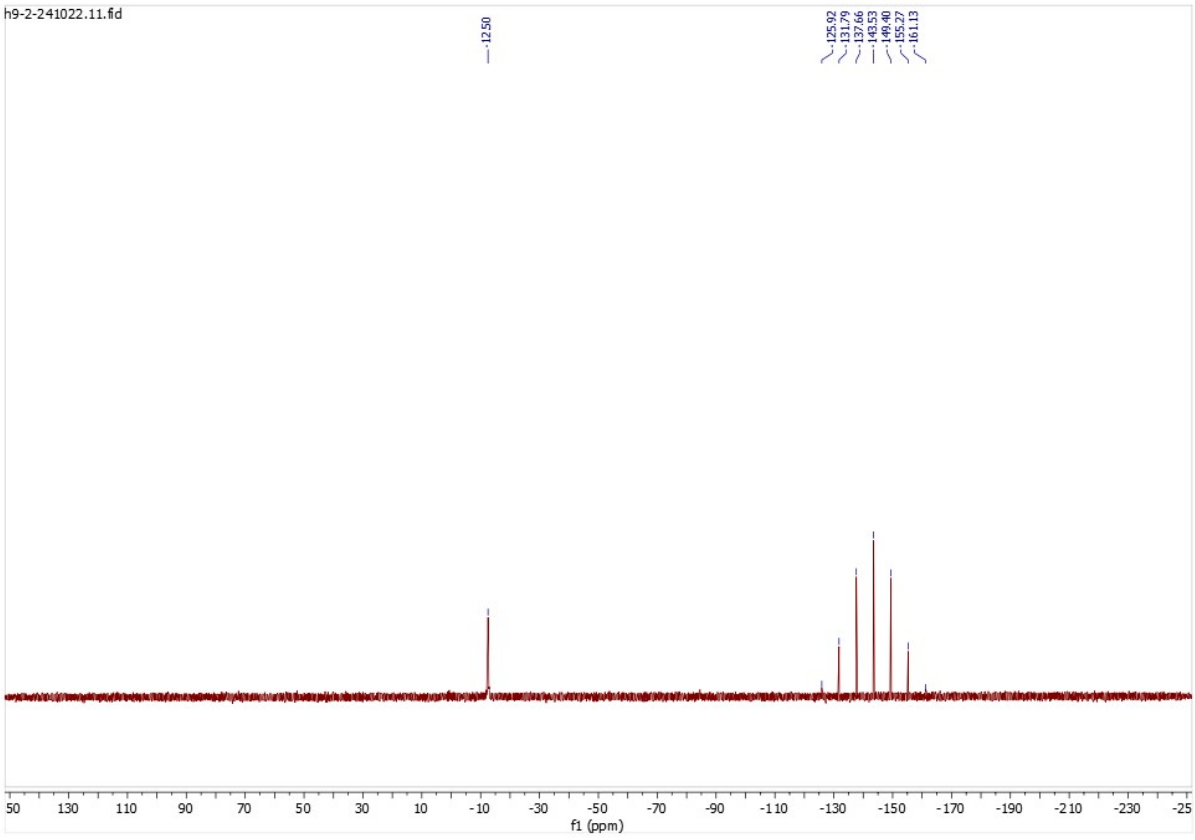

Figure S9. $^{31}P\{^{1}H\}$ NMR (121 MHz, CD_2Cl_2, 298 K) spectrum recorded for compound **Cu1.**

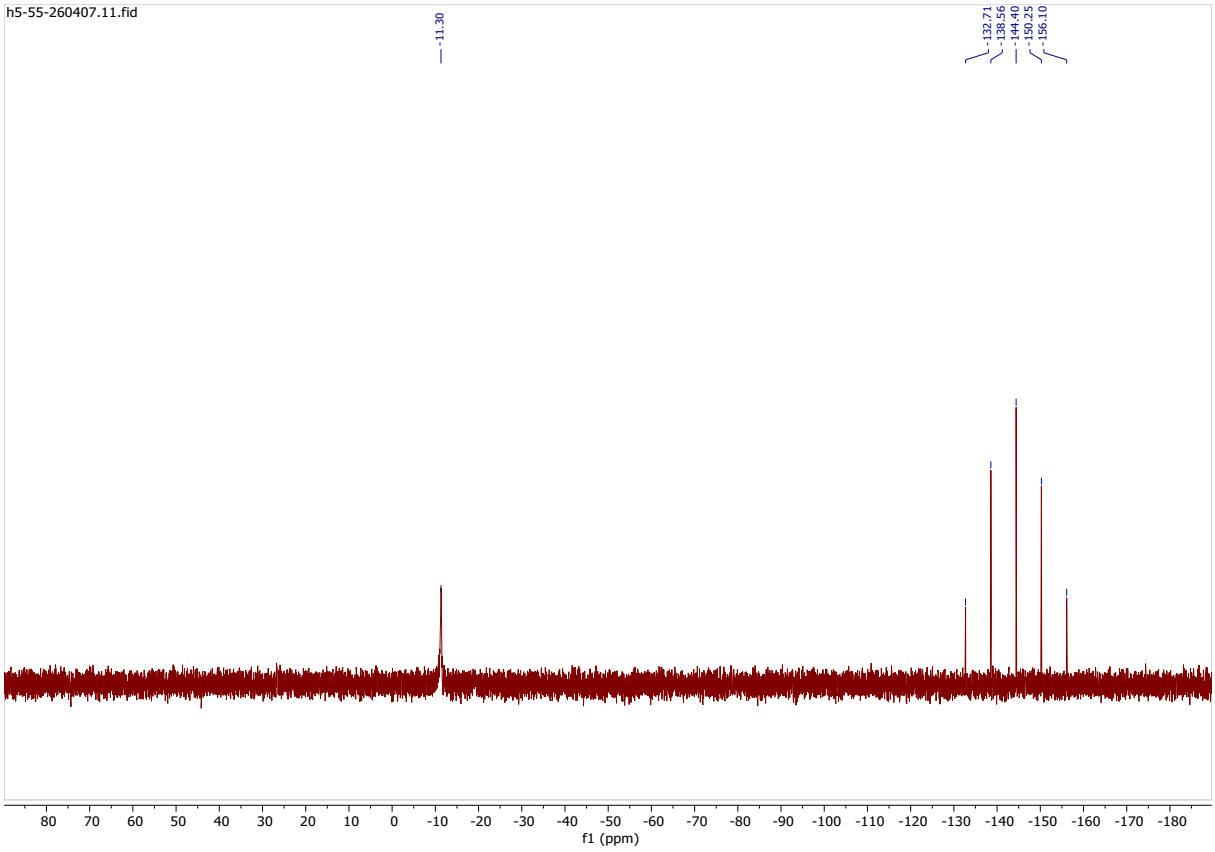

Figure S10. $^{31}P\{^{1}H\}$ NMR (121 MHz, CD_2Cl_2, 298 K) spectrum recorded for compound **Cu2.**

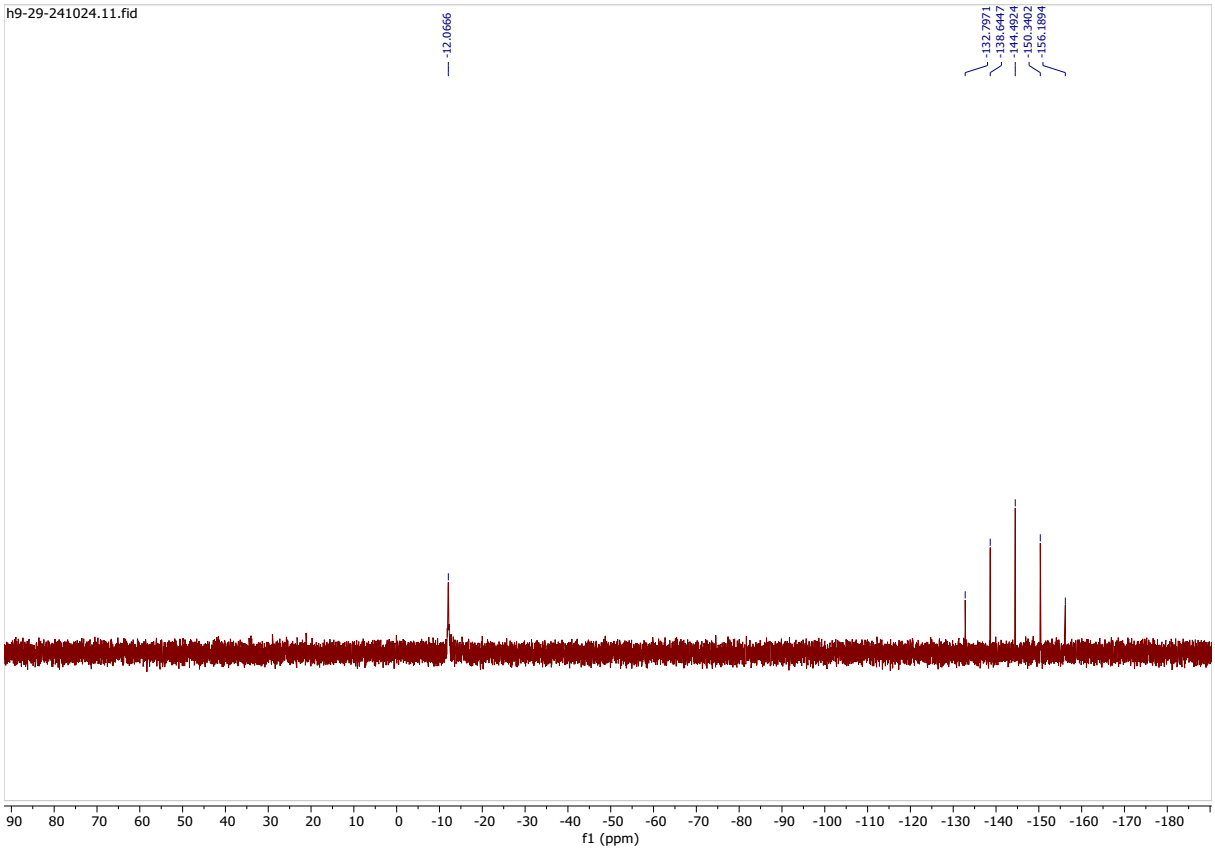

Figure S11. $^{31}P\{^{1}H\}$ NMR (121 MHz, CD_2Cl_2, 298 K) spectrum recorded for compound **Cu3.**

Figure S12. $^{31}P\{^{1}H\}$ NMR (121 MHz, CD_2Cl_2, 298 K) spectrum recorded for compound **Cu4**.

HR-MS-ESI spectra

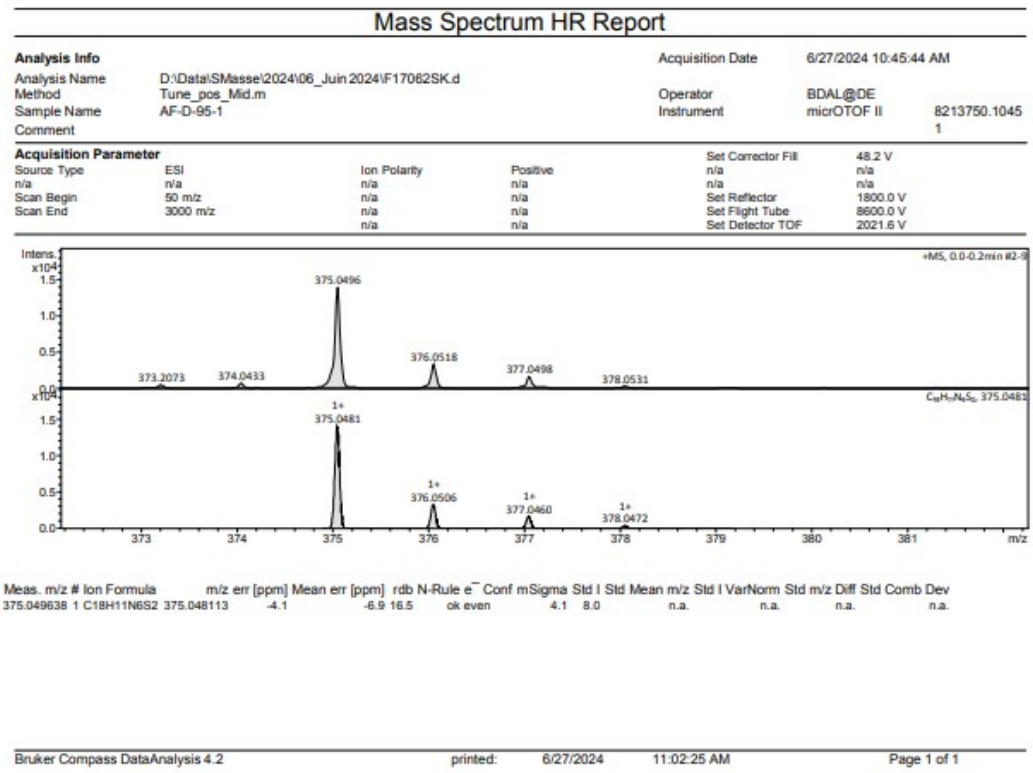

Mass Spectrum HR Report

Analysis Info

Analysis Name	D:\Data\SMasse\2024\06_Juin 2024\F17062SK.d	Acquisition Date	6/27/2024 10:45:44 AM
Method	Tune_pos_Mid.m	Operator	BDAL@DE
Sample Name	AF-D-95-1	Instrument	micrOTOF II 8213750.1045 1
Comment			

Acquisition Parameter

Source Type	ESI	Ion Polarity	Positive	Set Corrector Fill	48.2 V
n/a	n/a	n/a	n/a	n/a	n/a
Scan Begin	50 m/z	n/a	n/a	Set Reflector	1800.0 V
Scan End	3000 m/z	n/a	n/a	Set Flight Tube	8600.0 V
		n/a	n/a	Set Detector TOF	2021.6 V

Meas. m/z	#	Ion Formula	m/z err [ppm]	Mean err [ppm]	rdb	N-Rule	e⁻ Conf	mSigma	Std I	Std Mean m/z	Std I	VarNorm	Std m/z	Diff Std Comb	Dev
375.049638	1	C18H11N6S2	375.048113	-4.1	-6.9	16.5	ok	even	4.1	8.0	n.a.	n.a.	n.a.	n.a.	

Bruker Compass DataAnalysis 4.2 printed: 6/27/2024 11:02:25 AM Page 1 of 1

Figure S13. HR-ESI-MS spectrum recorded for compound **L1**.

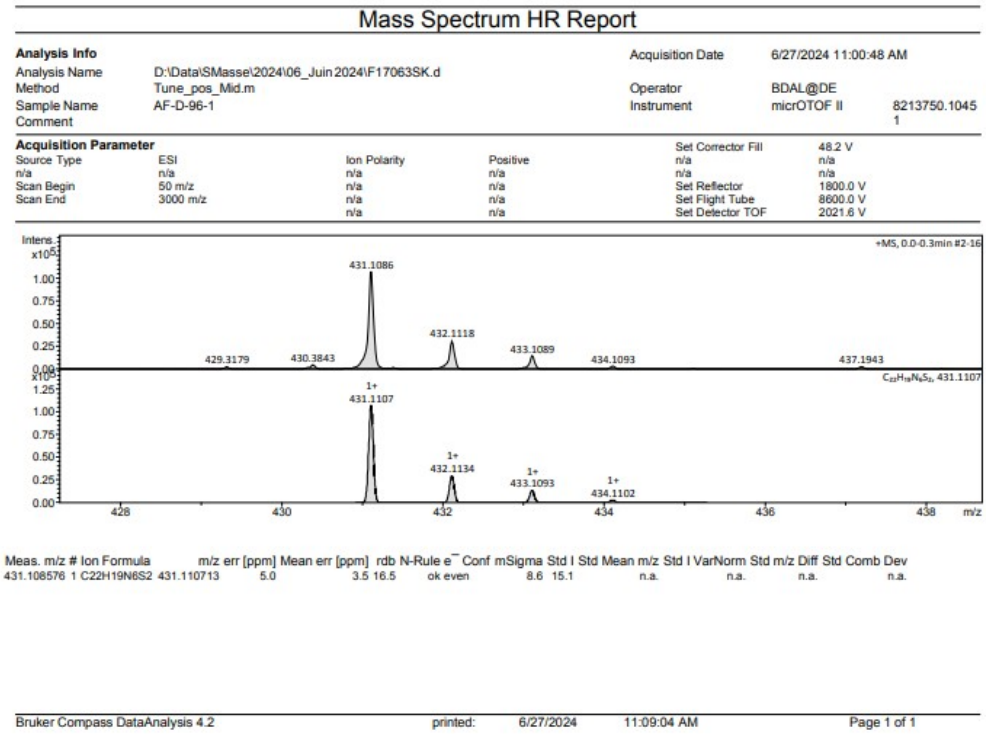

Figure S14. HR-ESI-MS spectrum recorded for compound **L2**.

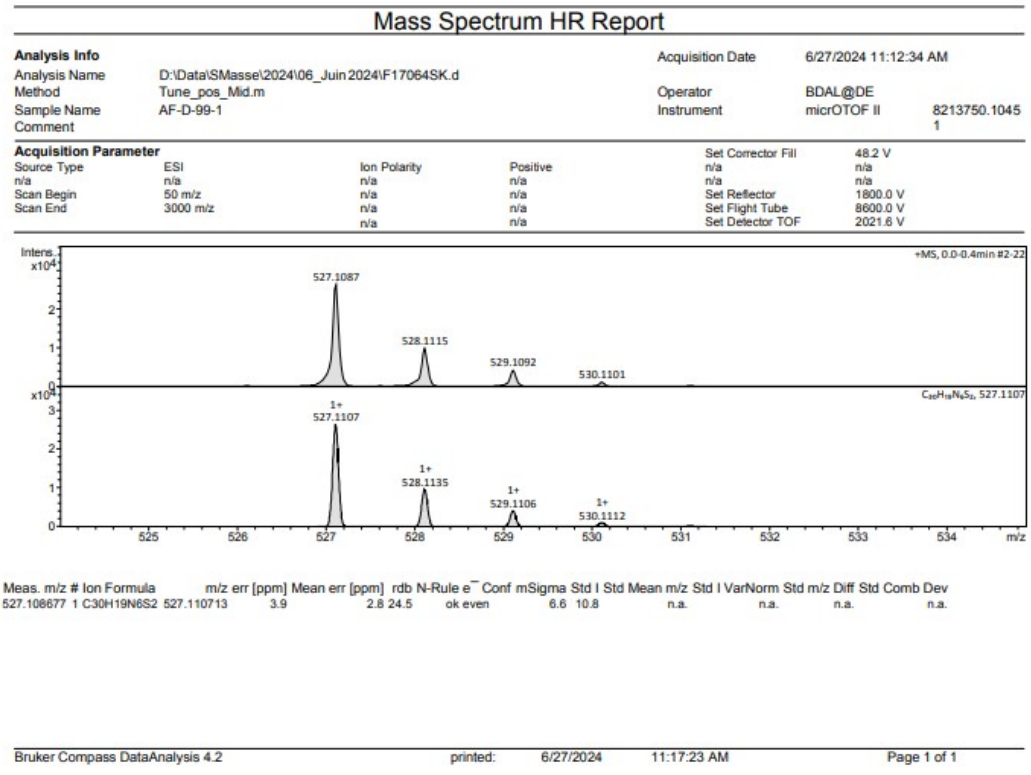

Figure S15. HR-ESI-MS spectrum recorded for compound **L3**.

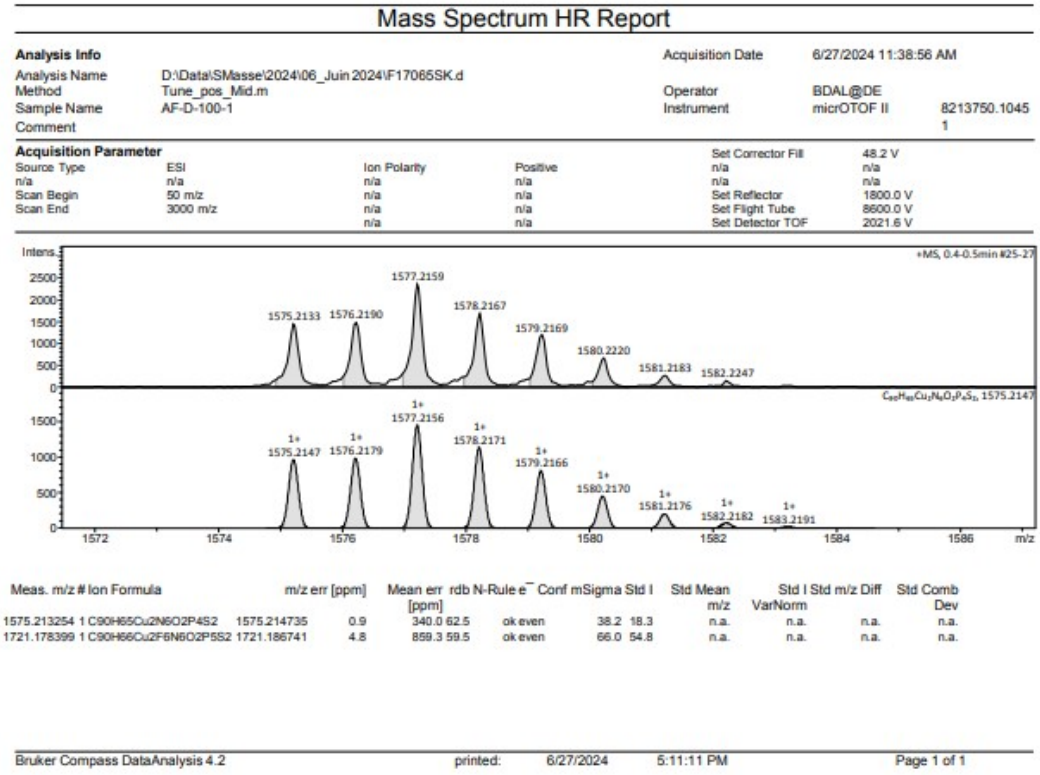

Figure S16. HR-ESI-MS spectrum recorded for compound **Cu1**.

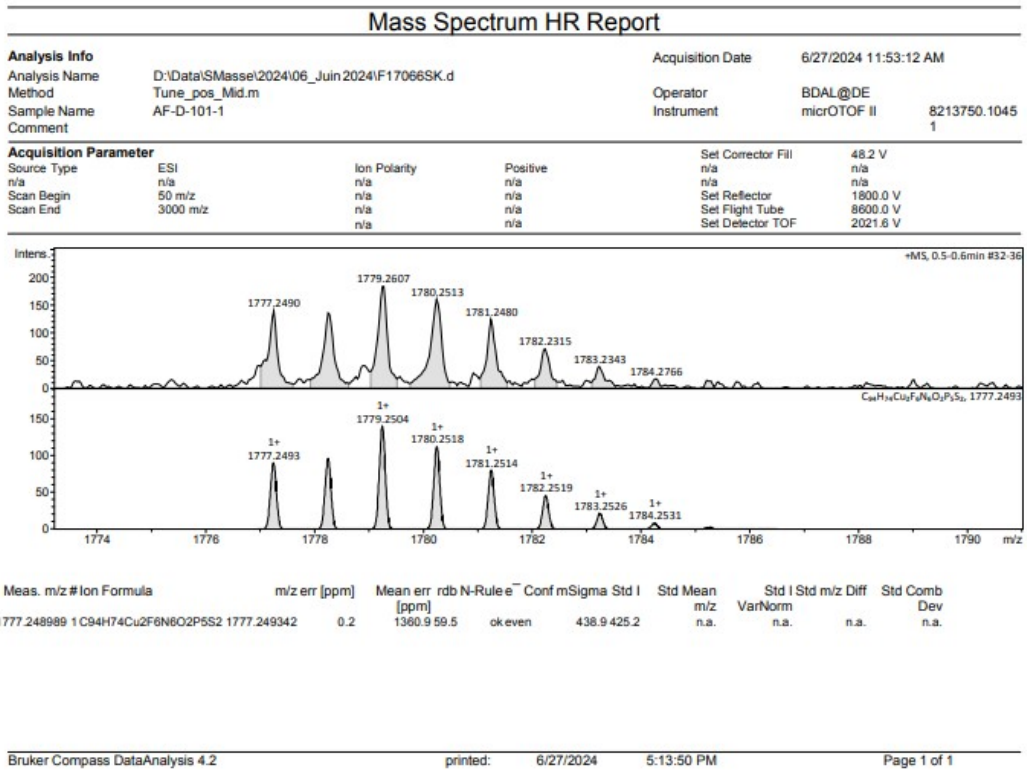

Figure S17. HR-ESI-MS spectrum recorded for compound **Cu2.**

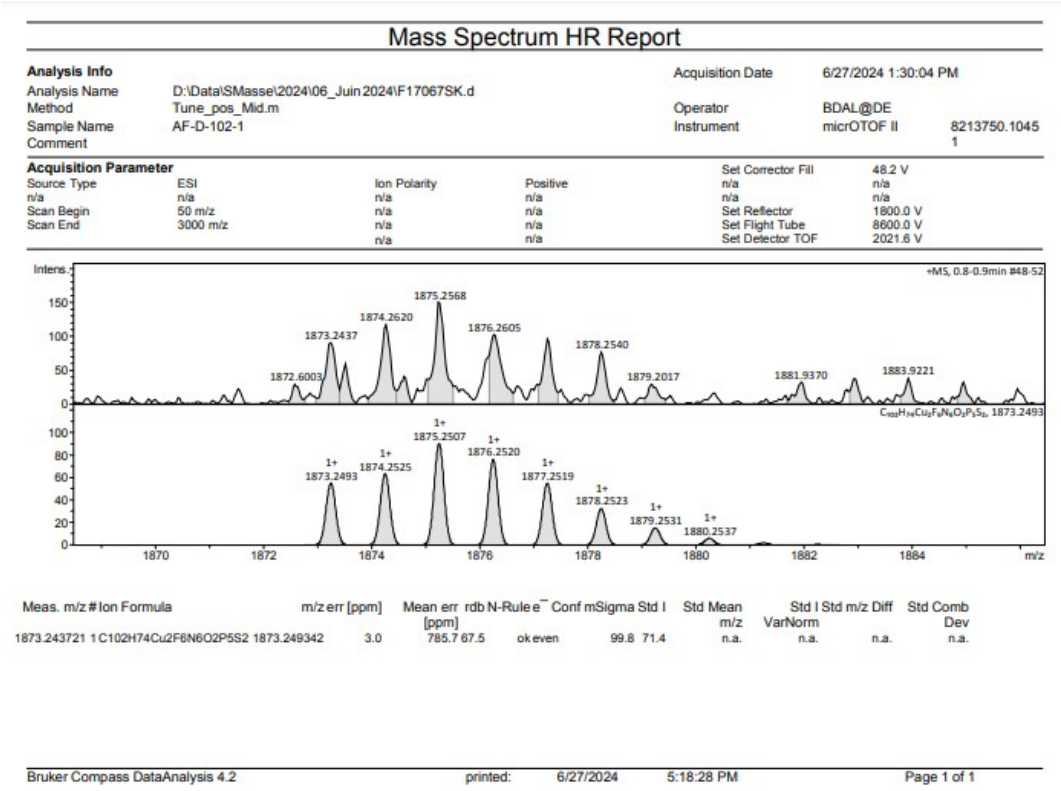

Figure S18. HR-ESI-MS spectrum recorded for compound **Cu3**.

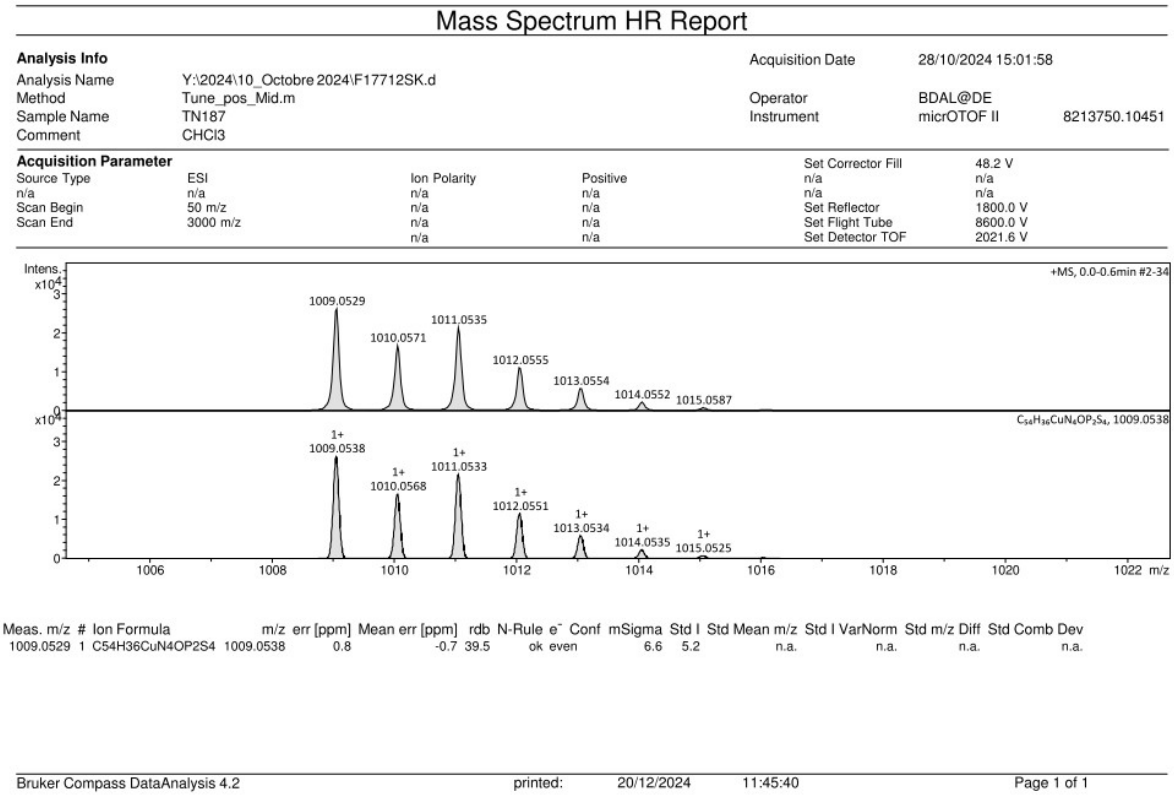

Figure S19. HR-ESI-MS spectrum recorded for compound **Cu4**.

Single crystal X-ray diffractometric analysis

Deposition numbers CCDC 2402732 (**L3**), 2402729 (**Cu1**), 2402730 (**Cu2**), 2402731 (**Cu3**), and CCDC 2412038 (**Cu4**) contain the supplementary crystallographic data for this paper. These data are provided free of charge by the joint Cambridge Crystallographic Data Centre and Fachinformationszentrum Karlsruhe *Access Structures* service.

For all compounds, X-ray diffraction data collection was carried out on a Bruker PHOTON-III DUO CPAD diffractometer equipped with an Oxford Cryosystem liquid N_2 device, using Mo-Kα radiation (λ = 0.71073 Å). The crystal-detector distance was 40 mm. The cell parameters were determined (APEX4 software)[2] from reflections taken from one set of 180 frames, each at 1 second exposure. The structures were solved using the program SHELXT-2018.[3] The refinement and all further calculations were carried out using SHELXL-2019.[4] The H-atoms were included in calculated positions and treated as riding atoms using SHELXL default parameters. The non-H atoms were refined anisotropically, using weighted full-matrix least-squares on *F*2. A semi-empirical absorption correction was applied using SADABS in APEX4[2]; transmission factors: T_{min}/T_{max} = 0.6970/0.7456. The SQUEEZE instruction in PLATON was applied.[5] The residual electron density was assigned to one molecule of solvent.

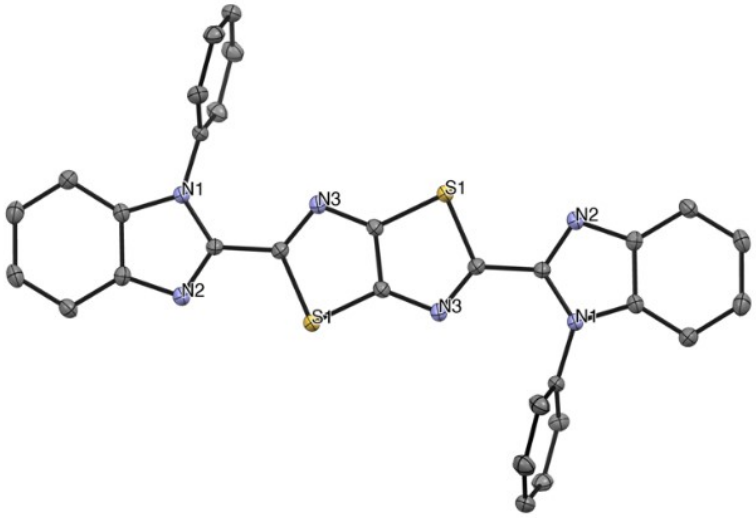

Figure S20. ORTEP diagram obtained for the ligand **L3** by means of single crystal X-ray diffractometric analysis. Thermal ellipsoids are shown at 50% probability level. Solvent molecules are omitted for clarity.

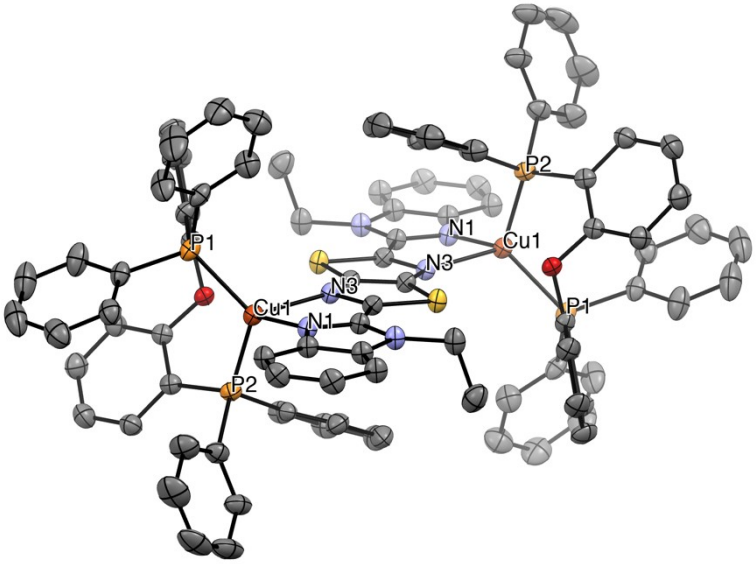

Figure S21. ORTEP diagram obtained for the complex **Cu2** by means of single crystal X-ray diffractometric analysis. Thermal ellipsoids are shown at 50% probability level. PF_6^- anions and solvent molecules are omitted for clarity.

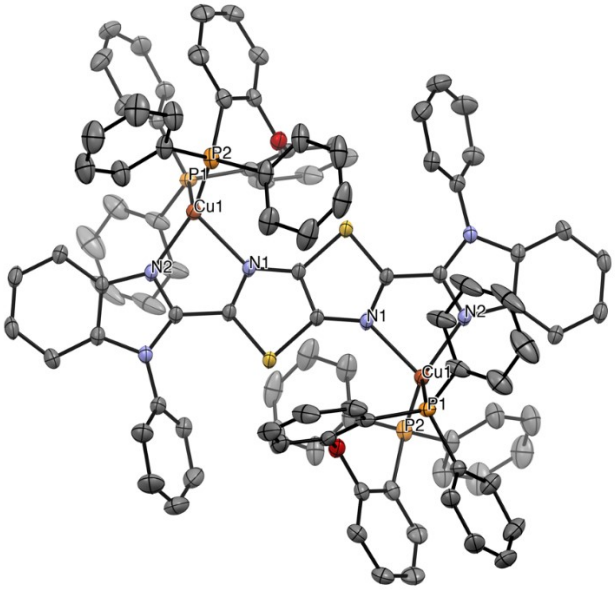

Figure S22. ORTEP diagram obtained for the complex **Cu3** by means of single crystal X-ray diffractometric analysis. Thermal ellipsoids are shown at 50% probability level. PF_6^- anions and solvent molecules are omitted for clarity.

Table S1. Crystal data and structure refinement for compound **L3** (CCDC 2402732).

Identification code	**eajaf240624**	
Empirical formula	$C_{32}H_{20}Cl_6N_6S_2$	
	$C_{30}H_{18}N_6S_2$,2($CHCl_3$)	
Formula weight	765.36	
Temperature	120(2) K	
Wavelength	0.71073 Å	
Crystal system, space group	Triclinic, P-1	
Unit cell dimensions	*a* = 9.6871(3) Å	α = 62.7580(10)°
	b = 10.3449(3) Å	β = 64.7870(10)°
	c = 10.6679(4) Å	γ = 65.5400(10)°
Volume	827.42(5) $Å^3$	
Z, Calculated density	1, 1.536 Mg/m^3	
Absorption coefficient	0.680 mm^{-1}	
F(000)	388	
Crystal size	0.180 x 0.080 x 0.080 mm	
Theta range for data collection	2.245 to 27.941°.	
Limiting indices	-12<=h<=12, -13<=k<=13, -14<=l<=14	
Reflections collected / unique	33923 / 3962 [R(int) = 0.0420]	
Completeness to theta = 25.242	99.9%	
Absorption correction	Semi-empirical from equivalents	
Max. and min. transmission	0.7456 and 0.7074	
Refinement method	Full-matrix least-squares on F^2	
Data / restraints / parameters	3962 / 0 / 208	
Goodness-of-fit on F^2	020	
Final R indices [I>2sigma(I)]	R1 = 0.0363, wR2 = 0.0836	
R indices (all data)	R1 = 0.0464, wR2 = 0.0903	
Extinction coefficient	n/a	
Largest diff. peak and hole	0.734 and -0.693 *e* $Å^{-3}$	

Table S2. Crystal data and structure refinement for compound **Cu1** (CCDC 2402729).

Identification code	**eajaf240619_02**	
Empirical formula	$C_{191}\ H_{158}Cu_4F_{24}N_{12}O_7P_{12}S_4$	
	$2(C_{90}H_{66}Cu_2N_6O_2\ P_4S_2)$, $4(F_6P)$, C_3H_6O, $2(C_4H_{10}O)$	
Formula weight	3943.32	
Temperature	120(2) K	
Wavelength	0.71073 Å	
Crystal system, space group	Orthorhombic, P b c a	
Unit cell dimensions	*a* = 20.6107(6) Å	α = 90°
	b = 20.4616(6) Å	β = 90°
	c = 42.7737(15) Å	γ = 90°
Volume	18038.9(10) $Å^3$	
Z, Calculated density	4, 1.452 Mg/m^3	
Absorption coefficient	0.704 mm^{-1}	
F(000)	8080	
Crystal size	0.200 x 0.140 x 0.120 mm	
Theta range for data collection	1.991 to 27.912°.	
Limiting indices	-27<=h<=27, -26<=k<=26, -56<=l<=56	
Reflections collected / unique	485640 / 21578 [R(int) = 0.0880]	
Completeness to theta = 25.242	100.0%	
Absorption correction	Semi-empirical from equivalents	
Max. and min. transmission	0.7456 and 0.7107	
Refinement method	Full-matrix least-squares on F^2	
Data / restraints / parameters	21578 / 3 / 1157	
Goodness-of-fit on F^2	002	
Final R indices [I>2	R1 = 0.0715, wR2 = 0.1310	
Extinction coefficient	n/a	
Largest diff. peak and hole	1.244 and -1.097 *e* $Å^{-3}$	

Table S3. Crystal data and structure refinement for compound **Cu2** (CCDC 2402730).

Identification code	**eajaf240618**	
Empirical formula	$C_{98}H_{80}Cl_{10}Cu_2F_{12}N_6O_2P_6S_2$	
	$C_{94}H_{74}Cu_2N_6O_2P_4S_2$, 2($F_6P$), 2($CHCl_3$), 2($CH_2Cl_2$)	
Formula weight	2333.20	
Temperature	120(2) K	
Wavelength	0.71073 Å	
Crystal system, space group	Monoclinic, P 21/c	
Unit cell dimensions	*a* = 13.5566(5) Å	α = 90°
	b = 13.1464(4) Å	β = 102.5990(10)°
	c = 29.0943(10) Å	γ = 90°
Volume	5060.3(3) Å^3	
Z, Calculated density	2, 1.531 Mg/m^3	
Absorption coefficient	0.895 mm^{-1}	
F(000)	2368	
Crystal size	0.200 x 0.120 x 0.060 mm	
Theta range for data collection	2.111 to 27.956°.	
Limiting indices	17<=h<=17, -17<=k<=17, -38<=l<=38	
Reflections collected / unique	279045 / 12142 [R(int) = 0.0853]	
Completeness to theta = 25.242	99.9%	
Absorption correction	Semi-empirical from equivalents	
Max. and min. transmission	0.7456 and 0.6862	
Refinement method	Full-matrix least-squares on F^2	
Data / restraints / parameters	12142 / 21 / 625	
Goodness-of-fit on F^2	1.024	
Final R indices [I>2sigma(I)]	R1 = 0.0798, wR2 = 0.2081	
R indices (all data)	R1 = 0.1005, wR2 = 0.2266	
Extinction coefficient	0.0042(5)	
Largest diff. peak and hole	1.799 and -1.921 *e* Å^{-3}	

Table S4. Crystal data and structure refinement for compound **Cu3** (CCDC 2402731).

Identification code	**eajaf240619sq**	
Empirical formula	$C_{108}H_{86}Cu_2F_{12}N_6O_4P_6S_2$, solvent	
	$C_{102}H_{74}Cu_2N_6O_2P_4S_2$, 2($F_6P$), 2($C_3H_6O$), solvent	
Formula weight	2136.84	
Temperature	120(2) K	
Wavelength	0.71073 Å	
Crystal system, space group	Triclinic, P -1	
Unit cell dimensions	*a* = 12.2112(3) Å	α = 87.6250(10)°
	b = 14.9814(5) Å	β = 69.3170(10)°
	c = 15.6492(5) Å	γ = 86.6330(10)°
Volume	2673.08(14) $Å^3$	
Z, Calculated density	1, 1.327 Mg/m^3	
Absorption coefficient	0.600 mm^{-1}	
F(000)	1096	
Crystal size	0.180 x 0.140 x 0.080 mm	
Theta range for data collection	1.925 to 27.939°.	
Limiting indices	-16<=h<=15, -19<=k<=19, -20<=l<=20	
Reflections collected / unique	99913 / 12801 [R(int) = 0.0373]	
Completeness to theta = 25.242	100.0%	
Absorption correction	Semi-empirical from equivalents	
Max. and min. transmission	0.7456 and 0.7115	
Refinement method	Full-matrix least-squares on F^2	
Data / restraints / parameters	12801 / 6 / 633	
Goodness-of-fit on F^2	1.026	
Final R indices [I>2sigma(I)]	R1 = 0.0539, wR2 = 0.1458	
R indices (all data)	R1 = 0.0611, wR2 = 0.1524	
Extinction coefficient	n/a	
Largest diff. peak and hole	1.770 and -1.240 *e* $Å^{-3}$	

Table S5. Crystal data and structure refinement for compound **Cu4** (CCDC 2412038).

Identification code	eajaj231214sq	
Empirical formula	C90 H64 Cu2 F12 N4 O2 P6 S4, solvent	
	C90 H64 Cu2 N4 O2 P4 S4, 2(F6 P) [+ solvent]	
Formula weight	1902.59	
Temperature	293(2) K	
Wavelength	1.54178 A	
Crystal system, space group	Orthorhombic, Pccn	
Unit cell dimensions	a = 14.7964(13) Å	α = 90°
	b = 20.192(2) Å	β = 90°
	c = 31.462(3) Å	γ = 90°
Volume	9400.1(15) $Å^3$	
Z, Calculated density	4, 1.344 Mg/ m^3	
Absorption coefficient	2.958 mm^{-1}	
F(000)	3872	
Crystal size	0.150 x 0.130 x 0.120 mm	
Theta range for data collection	2.809 to 66.597°g.	
Limiting indices	-17<=h<=12, -24<=k<=24, -36<=l<=37	
Reflections collected / unique	48088 / 8314 [R(int) = 0.1527]	
Completeness to theta = 66.597	100.0%	
Absorption correction	Semi-empirical from equivalents	
Max. and min. transmission	0.7528 and 0.2776	
Refinement method	Full-matrix least-squares on F^2	
Data / restraints / parameters	8314 / 29 / 506	
Goodness-of-fit on F^2	1.035	
Final R indices [I>2sigma(I)]	R1 = 0.0803, wR2 = 0.2186	
R indices (all data)	R1 = 0.1411, wR2 = 0.2635	
Extinction coefficient	n/a	
Largest diff. peak and hole	0.875 and -1.039 *e* A^{-3}	

Photophysical measurements

Instrument details. Absorption spectra were recorded using a Perkin Elmer Lambda 950 double-beam UV-VIS spectrophotometer and baseline corrected. Steady-state emission spectra were recorded on a Horiba Jobin−Yvon IBH FL-322 Fluorolog 3 spectrometer equipped with a 450 W xenon arc lamp, double-grating excitation, and emission monochromators (2.1 nm mm^{-1} of dispersion; 1200 grooves mm^{-1}) and a Hamamatsu R13456 red sensitive Peltier-cooled PMT detector. Emission and excitation spectra were corrected for source intensity (lamp and grating) and emission spectral response (detector and grating) by standard correction curves. Time-resolved measurements were performed using either the Time-Correlated Single-Photon Counting (TCSPC) or the Multi-Channel Scaling (MCS) electronics option of the TimeHarp 260 board installed on a PicoQuant FluoTime 300 fluorimeter (PicoQuant GmbH, Germany), equipped with a PDL 820 laser pulse driver. A pulsed laser diode LDH-P-C-375 (λ = 375 nm, pulse full width at half maximum <50 ps, repetition rate 200 kHz–40 MHz) was used to excite the sample and mounted directly on the sample chamber at 90°. The photons were collected by a PMA Hybrid-07 single photon counting detector. The data were acquired by using the commercially available software EasyTau II (PicoQuant GmbH, Germany), while data analysis was performed using the built-in software FluoFit (PicoQuant GmbH, Germany). All the solvents were spectrophotometric grade. Dearated samples were prepared by the freeze–pump–thaw technique by using a home-made quartz cuvette equipped with a Rotaflo stopcock. Luminescence quantum yields were measured in optically dilute solutions (optical density <0.15 at the excitation wavelength) and compared to reference emitter by following the method of Demas and Crosby.[6] The $Ru(bpy)_3Cl_2$ complex in air-equilibrated water solution at room temperature was used as reference (PLQY = 0.04).[7] Solid state PLQY values were recorded at a fixed excitation wavelength by using a Hamamatsu Photonics absolute PLQY measurements system Quantaurus QY equipped with CW Xenon light source (150 W), monochromator, integrating sphere, C7473 photonics multi-channel analyzer and employing the commercially available U6039-05 PLQY measurement software (Hamamatsu Photonics Ltd., Shizuoka, Japan). All measurements were repeated four times at the excitation wavelength λ_{exc} = 360 nm, unless otherwise stated.

Methods. For time resolved measurements, data fitting was performed by employing the maximum likelihood estimation (MLE) methods and the quality of the fit was assessed by inspection of the reduced χ^2 function and of the weighted residuals. For multi-exponential

decays, the intensity, namely I*(t)*, has been assumed to decay as the sum of individual single exponential decays (Eqn. 1):

$$I(t) = \sum_{i=1}^{n} \alpha_i exp\left(-\frac{t}{\tau_i}\right) \qquad \text{eqn. 1}$$

where τ_i are the decay times and α_i are the amplitude of the component at $t = 0$. In the tables, the percentages to the pre-exponential factors, α_i, are listed upon normalization. Intensity average lifetimes were calculated by using the following equation (Eqn. 2):[8]

$$\bar{\tau} = \frac{a_1\tau_1^2 + a_2\tau_2^2}{a_1\tau_1 + a_2\tau_2} \qquad \text{eqn. 2}$$

Table S6. Photophysical data recorded for ligands **L1**–**L4** as neat powders and DCM glassy matrix at 77 K.

cmpd	λ_{em} [nm]		PLQY (%)	τ_{obs} ($\%A_{rel}$)		$\bar{\tau}$ [ns]		k_r [10^8 s^{-1}]	k_{nr} [10^8 s^{-1}]
	powder	77 K	powder	powder	77 K	powder	77 K		
L1	524*sh*, 566*sh*, **596**	436, **465**, 497, 535*sh*	2	1.03 (52%) 0.36 (48%)	1.29	0.87	-	0.22	11.2
L2	497*sh*, 525*sh*, **551**	442, **468**, 501, 536*sh*	24	1.68 (52%) 0.70 (48%)	1.32	1.42	-	1.69	5.36
L3	500*sh*, 529*sh*, **555**	441, 472, **511**, 556*sh*	41	2.66 (35%) 1.29 (65%)	1.59	2.01	-	2.03	2.92
L4	510*sh*, **552**, 594, 644*sh*	363, **382**, 404	13	2.46 (55%) 0.82 (45%)	0.994 (64%) 2.33 (26%)	2.11	1.68	0.61	4.12

sh denotes a shoulder.

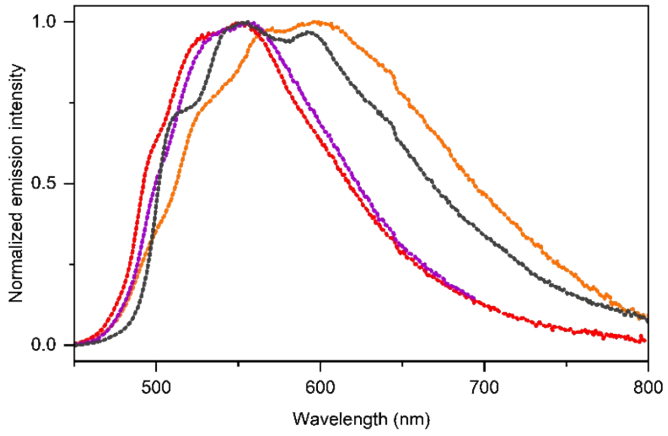

Figure S23. Emission spectra of ligands **L1** (orange), **L2** (red), **L3** (violet), and **L4** (grey) in the solid state as neat powders at room temperature upon excitation at λ_{exc} = 420 nm.

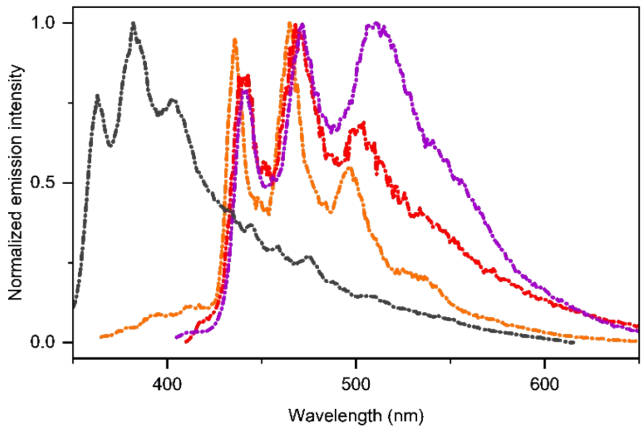

Figure S24. Emission spectra of ligands **L1** (orange), **L2** (red), **L3** (violet), and **L4** (grey) in CH_2Cl_2 glassy matrix at 77K upon excitation at λ_{exc} = 320–380 nm.

Electrochemical characterization

The electrochemical properties of the complexes were assessed by means of cyclic voltammetry (CV). The CV experiments were carried out using a three-electrode electrochemical cell in anhydrous and degassed dichloromethane (DCM)/0.1M $TBAPF_6$ solution under an Ar atmosphere, using a 1 mM concentration for the copper complexes. Tetra-n-butylammonium hexafluorophosphate ($TBAPF_6$, Sigma-Aldrich, 99%) was used at the supporting electrolyte and employed as received. The working electrode was a glassy-carbon (GC) disk electrode (2 mm diameter, PAR-Ametek). The electrode was polished as already described elsewhere.[9] Before experiments, the electrode was further polished with a 0.05 mm polycrystalline diamond suspension (Buehler, MetaDi) and electrochemically activated in the background solution by means of several voltammetric cycles at 0.5 Vs^{-1} between the anodic and the cathodic solvent/electrolyte discharges, until the expected quality features were attained.[10] A platinum wire served as the counter electrode, while a silver wire, separated by the catolyte solution by a vycor frit, was used as a quasi-reference electrode. At the end of each experiment, the potential of the reference electrode was calibrated against the ferricenium/ferrocene ($Fc^+|Fc^0$) couple, used as the internal redox standard. The solvent level was frequently checked and rinsed when necessary to avoid any change in the analyte concentration. An SP300 (Biologic) was used as the workstation for the CV experiments. A feedback compensation was applied to overcome the ohmic drop of the potential at the interface

electrode/solution. The effect of the scan rate was investigated over the range 50–500 mV s^{-1}, and the peak current was found to depend linearly on the square root of scan rate for all compound, thus witnessing that the heterogeneous electron transfer process is diffusion-controlled. It is also worth noting that the peak-to-peak separation for all compound is in the range 60-70 mV, which is slightly larger than 59 mV expected for an ideal Nernstian behavior[11], thus indicating a slightly slower kinetic for the heterogeneous electron transfer when compared to $Fc^{+}|Fc^{0}$ redox couple.

Computational data

All calculation were made using the AMS-2024 code[12,13] at the density functional theory with B3LYP functional (DFT).[14] All atoms were described with the DZP basis-set.[15] Scalar relativistic were introduced through the zero-order relativistic approximation (ZORA) Hamiltonian.[16] All calculations were made with a non-explicit dichloromethane solvent within the Conductor-like-screening model (COSMO).[17] Weak interactions were introduced through Grimme D3 corrections.[18] The structures of all complexes were fully optimized and the absorption spectra computed through time dependent DFT (TD-DFT) using the Tamm-Dancoff approximation (TDA).[19] Spin-orbit coupling corrections were introduced by perturbation of the computed spectra. Emission properties were determined after the optimization of excited states geometries through the TD-DFT approach, in the same conditions. The nature of the excited states has been analyzed with TheoDORE software.[20] The electron density differences were computed using the dgrid package and visualized using ChimeraX software.[21]

Non-Covalent Interaction (NCI) analyses have been performed by computing the wavefunction of the complexes with GAUSSIAN 16 (version C01)[22] at DFT level of Theory (B3LYP functional)[23] with the inclusion of Grimme's (GD3) dispersion corrections.[18] All atoms were described by Pople's 6-31+G** basis set.[24] The solvent (CH_2Cl_2) was introduced through a PCM.[25] The NCI analysis was then done on the results wavefunction using the NCIplot package.[26]

Table S7. Compared theoretical and experimental structures. Distances are given in [Å]. N_{az} = nitrogen of the thiazolo[4,5-*d*]thiazole moiety, N_{py} = nitrogen of the peripheral moiety. Cu(1), Cu(2), P(1), and P(2) follow the atom numbering depicted in Figure 1 of the main text.

	Cu1	**Cu2**	**Cu3**	**Cu4**

	Exp	Theo	Exp	Theo	Exp	Theo	Exp	Theo
Cu(1)–N_{az}	2.014	2.040	2.018	2.053	2.050	2.063	2.100	2.069
Cu(1)–N_{py}	2.136	2.265	2.195	2.203	2.131	2.159	2.120	2.131
Cu(1)–P(1)	2.220	2.256	2.217	2.227	2.214	2.207	2.212	2.211
Cu(1)–P(2)	2.239	2.217	2.252	2.260	2.279	2.278	2.262	2.272
Cu(2)–N_{az}	2.014	2.038	2.018	2.037	2.050	2.063	2.100	2.069
Cu(2)–N_{py}	2.136	2.367	2.195	2.311	2.126	2.159	2.120	2.131
Cu(2)–P(1)	2.220	2.220	2.217	2.221	2.211	2.207	2.212	2.211
Cu(2)–P(2)	2.239	2.260	2.252	2.076	2.267	2.278	2.262	2.272

Table S8. Absorption energies, absorption wavelength and oscillator strength of the first 20 computed singlet transitions for pro-ligands **L1-4**. Energies and wavelengths are given in [eV] and [nm], respectively.

	L1			**L2**			**L3**			**L4**		
	E_{abs}	λ_{abs}	f_{osc}	E_{abs}	λ_{abs}	f_{osc}	E_{abs}	λ_{abs}	f_{osc}	E_{abs}	λ_{abs}	f_{osc}
S_1	2.947	421	2.22E+00	2.929	423	2.17E+00	2.961	419	2.24E+00	2.820	440	2.13E+00
S_2	3.716	334	4.02E-02	3.648	340	9.30E-06	3.674	337	1.22E-02	3.482	356	7.13E-02
S_3	3.719	333	5.96E-08	3.650	340	6.96E-02	3.684	337	5.41E-02	3.492	355	3.79E-08
S_4	3.816	325	2.68E-07	3.812	325	9.06E-08	3.820	325	1.09E-04	3.766	329	4.10E-07
S_5	4.059	305	2.76E-07	4.040	307	8.70E-07	4.089	303	1.40E-03	3.884	319	1.64E-06
S_6	4.276	290	1.97E-01	4.247	292	2.18E-01	4.120	301	1.40E-01	4.032	307	2.29E-01
S_7	4.659	266	1.96E-06	4.483	277	2.11E-07	4.314	287	1.19E-04	4.406	281	3.77E-07
S_8	4.756	261	1.40E-01	4.726	262	1.35E-01	4.331	286	7.67E-03	4.478	277	3.08E-08
S_9	4.801	258	1.83E-07	4.730	262	5.39E-05	4.388	283	1.35E-04	4.488	276	1.03E-01
S_{10}	4.814	258	3.40E-02	4.760	260	6.52E-02	4.393	282	1.63E-05	4.499	276	2.90E-06
S_{11}	4.895	253	1.61E-03	4.816	257	4.23E-07	4.432	280	2.21E-04	4.520	274	5.96E-04
S_{12}	4.896	253	1.50E-01	4.849	256	2.29E-03	4.443	279	2.62E-03	4.588	270	1.85E-02
S_{13}	4.922	252	2.74E-03	4.890	254	1.38E-01	4.593	270	3.40E-02	4.817	257	1.29E-01
S_{14}	5.014	247	3.81E-07	5.002	248	5.27E-07	4.661	266	4.43E-02	5.029	247	3.80E-08
S_{15}	5.176	240	4.81E-02	5.118	242	5.51E-02	4.694	264	5.90E-04	5.036	246	1.55E-01
S_{16}	5.297	234	1.96E-08	5.235	237	8.55E-04	4.732	262	7.56E-02	5.054	245	1.46E-08
S_{17}	5.362	231	1.46E-08	5.258	236	3.95E-07	4.780	259	6.14E-02	5.076	244	4.88E-06
S_{18}	5.378	231	1.64E-05	5.339	232	2.67E-08	4.794	259	6.12E-02	5.130	242	1.81E-05
S_{19}	5.547	224	4.76E-05	5.456	227	3.50E-04	4.904	253	2.31E-02	5.247	236	4.17E-08
S_{20}	5.583	222	3.62E-08	5.465	227	1.37E-07	4.911	252	1.13E-01	5.247	236	5.19E-03

Table S9. Comparison between the computed energies of the frontier orbitals of isolated ligand **L1** to **L4** and **Cu1** to **Cu4**. In red are the LUMO and in green the HOMO of the ligand and their equivalent TzTz orbitals in the complex. Values of the HOMO-LUMO gap ($\Delta_{H\text{-}L}$) and, for the complexes, gap ($\Delta_{L\text{-}L}$) between the LUMO and the highest HOMO purely localized on the TzTz ligand. Energies are given in [eV].

orbital	**L1**	**Cu1**	**L2**	**Cu2**	**L3**	**Cu3**	**L4**	**Cu4**
HOMO-4								-7.174
HOMO-3								-7.160
HOMO-2		-7.044		-6.999		-6.940		-7.091
HOMO-1		-6.642		-6.543		-6.518		-6.715
HOMO	-6.099	-6.599	-6.008	-6.438	-6.050	-6.422	-6.230	-6.673
LUMO	-2.714	-3.855	-2.641	-3.755	-2.692	-3.722	-2.972	-4.054
$\Delta_{H\text{-}L}$	***3.385***	***2.744***	***3.367***	***2.683***	***3.358***	***2.700***	***3.258***	***2.619***

Table S10. Absorption energies, absorption wavelength and oscillator strength of the first 50 computed singlet transitions for **Cu1-4**. Energies and wavelengths are given in [eV] and [nm], respectively.

	Cu1			**Cu2**			**Cu3**			**Cu4**		
	E_{abs}	λ_{abs}	f_{osc}	E_{abs}	λ_{abs}	f_{osc}	E_{abs}	λ_{abs}	f_{osc}	E_{abs}	λ_{abs}	f_{osc}
S_1	2.209	561	2.29E-01	2.161	574	1.22E-01	2.174	570	1.26E-01	2.100	590	2.13E-01
S_2	2.277	545	1.00E-03	2.266	547	5.35E-02	2.267	547	5.90E-02	2.164	573	1.70E-03

S_3	2.530	490	2.13E-03		2.739	453	9.06E-02		2.743	452	2.66E-03		2.372	523	2.60E-03
S_4	2.625	472	7.10E-03		2.800	443	6.60E-02		2.800	443	1.16E+00		2.469	502	9.17E-03
S_5	2.778	446	8.01E-01		2.827	439	8.51E-01		2.853	435	5.40E-01		2.647	468	1.12E-01
S_6	2.825	439	9.21E-01		2.884	430	6.41E-01		2.931	423	5.05E-03		2.699	459	8.52E-04
S_7	2.850	435	6.90E-04		3.017	411	7.33E-02		3.000	413	5.45E-02		2.737	453	1.60E+00
S_8	3.168	391	6.36E-04		3.094	401	1.39E-03		3.157	393	1.22E-02		2.993	414	6.80E-04
S_9	3.175	390	1.15E-02		3.143	394	4.83E-03		3.242	382	2.40E-02		2.999	413	1.24E-02
S_{10}	3.276	378	9.42E-04		3.230	384	4.41E-02		3.257	381	3.41E-02		3.082	402	1.49E-03
S_{11}	3.324	373	4.36E-02		3.281	378	1.49E-02		3.294	376	2.45E-02		3.113	398	1.05E-02
S_{12}	3.333	372	1.30E-01		3.345	371	6.57E-02		3.310	375	8.69E-04		3.128	396	4.14E-05
S_{13}	3.334	372	7.12E-06		3.375	367	5.57E-02		3.363	369	8.13E-02		3.131	396	2.07E-01
S_{14}	3.425	362	9.64E-04		3.532	351	4.55E-02		3.557	349	2.44E-03		3.303	375	6.40E-04
S_{15}	3.490	355	8.50E-03		3.550	349	2.57E-03		3.589	345	1.52E-02		3.318	374	1.20E-03
S_{16}	3.504	354	6.14E-04		3.571	347	5.74E-03		3.602	344	7.91E-03		3.320	373	4.53E-04
S_{17}	3.524	352	1.51E-02		3.583	346	5.17E-04		3.630	342	7.57E-03		3.322	373	2.67E-02
S_{18}	3.539	350	2.98E-03		3.609	344	4.33E-03		3.643	340	2.25E-03		3.358	369	2.59E-02
S_{19}	3.544	350	2.52E-02		3.623	342	2.40E-03		3.652	340	1.19E-02		3.358	369	2.10E-03
S_{20}	3.598	345	1.05E-04		3.632	341	2.50E-03		3.683	337	2.07E-02		3.404	364	1.08E-03
S_{21}	3.611	343	7.86E-03		3.663	338	7.25E-03		3.689	336	2.05E-02		3.437	361	2.46E-03
S_{22}	3.617	343	8.25E-04		3.686	336	9.33E-03		3.707	334	6.02E-03		3.443	360	5.10E-03
S_{23}	3.623	342	4.05E-03		3.703	335	3.25E-02		3.731	332	7.04E-03		3.453	359	2.66E-03
S_{24}	3.626	342	5.84E-04		3.731	332	1.34E-02		3.736	332	2.03E-03		3.461	358	6.20E-06
S_{25}	3.649	340	5.27E-04		3.733	332	1.25E-02		3.744	331	2.72E-02		3.469	357	4.61E-03
S_{26}	3.652	340	4.15E-02		3.738	332	1.48E-02		3.750	331	6.42E-03		3.487	356	7.69E-04
S_{27}	3.669	338	7.14E-03		3.744	331	1.20E-03		3.762	330	1.19E-02		3.493	355	1.16E-02
S_{28}	3.690	336	3.79E-05		3.766	329	4.86E-03		3.772	329	1.04E-02		3.512	353	1.01E-02
S_{29}	3.692	336	1.77E-02		3.776	328	2.33E-03		3.799	326	6.11E-03		3.523	352	3.51E-02
S_{30}	3.716	334	5.00E-04		3.787	327	7.72E-03		3.808	326	1.29E-02		3.529	351	2.01E-06
S_{31}	3.733	332	4.04E-04		3.830	324	2.43E-03		3.822	324	2.99E-03		3.555	349	5.52E-03
S_{32}	3.733	332	1.94E-02		3.835	323	2.32E-03		3.838	323	7.51E-03		3.565	348	1.64E-05
S_{33}	3.755	330	2.02E-03		3.846	322	9.71E-03		3.845	322	3.74E-02		3.567	348	2.98E-02
S_{34}	3.774	329	9.22E-03		3.871	320	8.60E-02		3.851	322	2.89E-03		3.632	341	4.30E-03
S_{35}	3.779	328	4.11E-03		3.883	319	2.73E-03		3.859	321	4.42E-03		3.633	341	2.64E-03
S_{36}	3.782	328	1.04E-02		3.884	319	2.76E-03		3.871	320	1.18E-02		3.658	339	2.19E-03
S_{37}	3.809	325	5.42E-03		3.901	318	2.48E-02		3.885	319	5.47E-02		3.694	336	5.23E-03
S_{38}	3.832	324	1.82E-03		3.914	317	1.98E-02		3.891	319	3.66E-02		3.728	333	3.37E-03
S_{39}	3.890	319	5.73E-03		3.930	315	4.93E-04		3.908	317	1.95E-02		3.772	329	7.71E-04
S_{40}	3.913	317	1.85E-03		3.962	313	7.65E-02		3.940	315	7.50E-02		3.774	328	1.03E-03
S_{41}	3.951	314	4.29E-03		3.974	312	1.83E-03		3.967	313	2.32E-03		3.782	328	1.59E-03
S_{42}	3.952	314	6.96E-04		3.981	311	8.17E-03		3.970	312	4.41E-03		3.790	327	6.63E-04
S_{43}	3.960	313	2.91E-05		4.004	310	2.61E-02		3.986	311	8.51E-03		3.843	323	8.98E-04
S_{44}	3.984	311	4.07E-04		4.009	309	6.21E-02		3.987	311	1.41E-02		3.845	322	4.96E-03
S_{45}	4.000	310	5.13E-04		4.024	308	1.00E-01		4.003	310	9.32E-03		3.849	322	1.93E-02
S_{46}	4.048	306	3.76E-03		4.039	307	4.17E-03		4.005	310	6.96E-02		3.972	312	2.98E-03
S_{47}	4.050	306	2.37E-01		4.050	306	5.78E-02		4.022	308	6.36E-02		4.000	310	3.91E-03
S_{48}	4.091	303	1.20E-02		4.053	306	1.88E-02		4.029	308	6.09E-03		4.003	310	8.40E-04
S_{49}	4.096	303	5.60E-03		4.056	306	8.46E-03		4.049	306	1.33E-02		4.012	309	2.69E-04
S_{50}	4.131	300	2.65E-02		4.107	302	3.26E-03		4.051	306	3.62E-03		4.078	304	1.39E-02

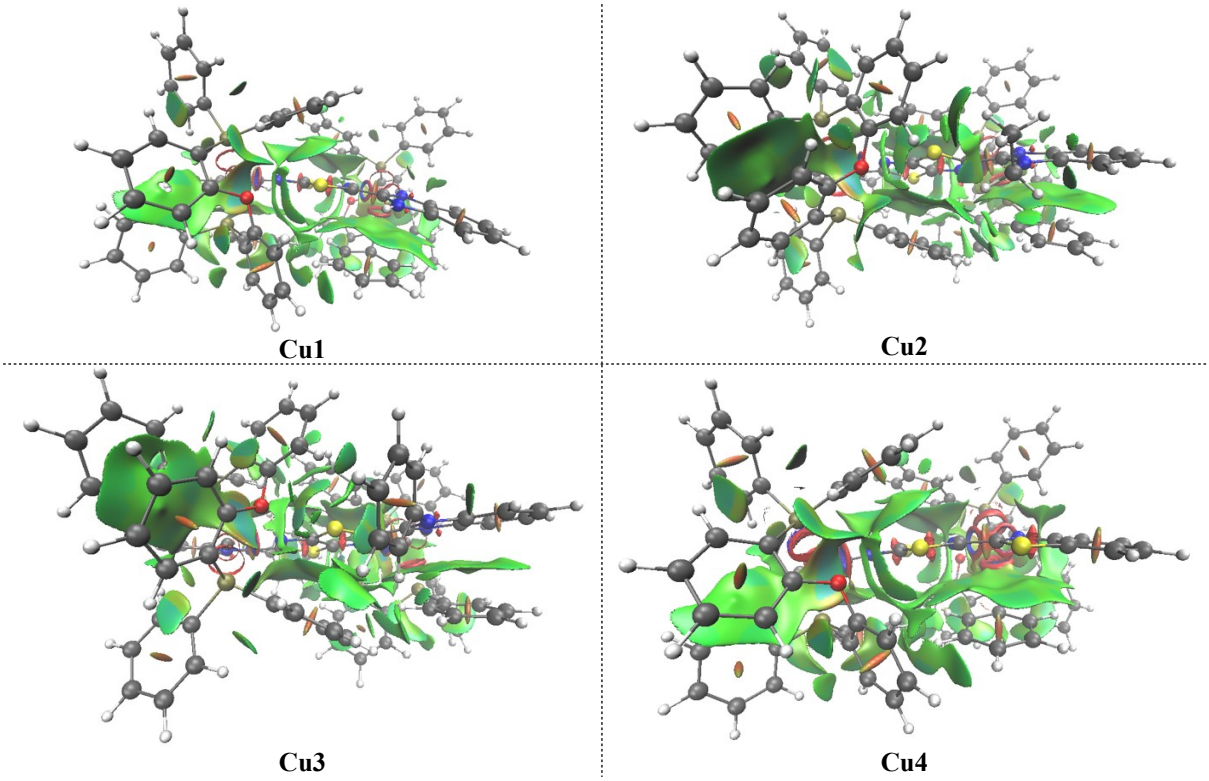

Figure S25. Non-Covalent Interaction (NCI) analysis of **Cu1**, **Cu2**, **Cu3** and **Cu4** complexes. Red areas correspond to repulsive steric interactions, green areas to attractive dispersions forces and blue areas to attractive electrostatic interactions.

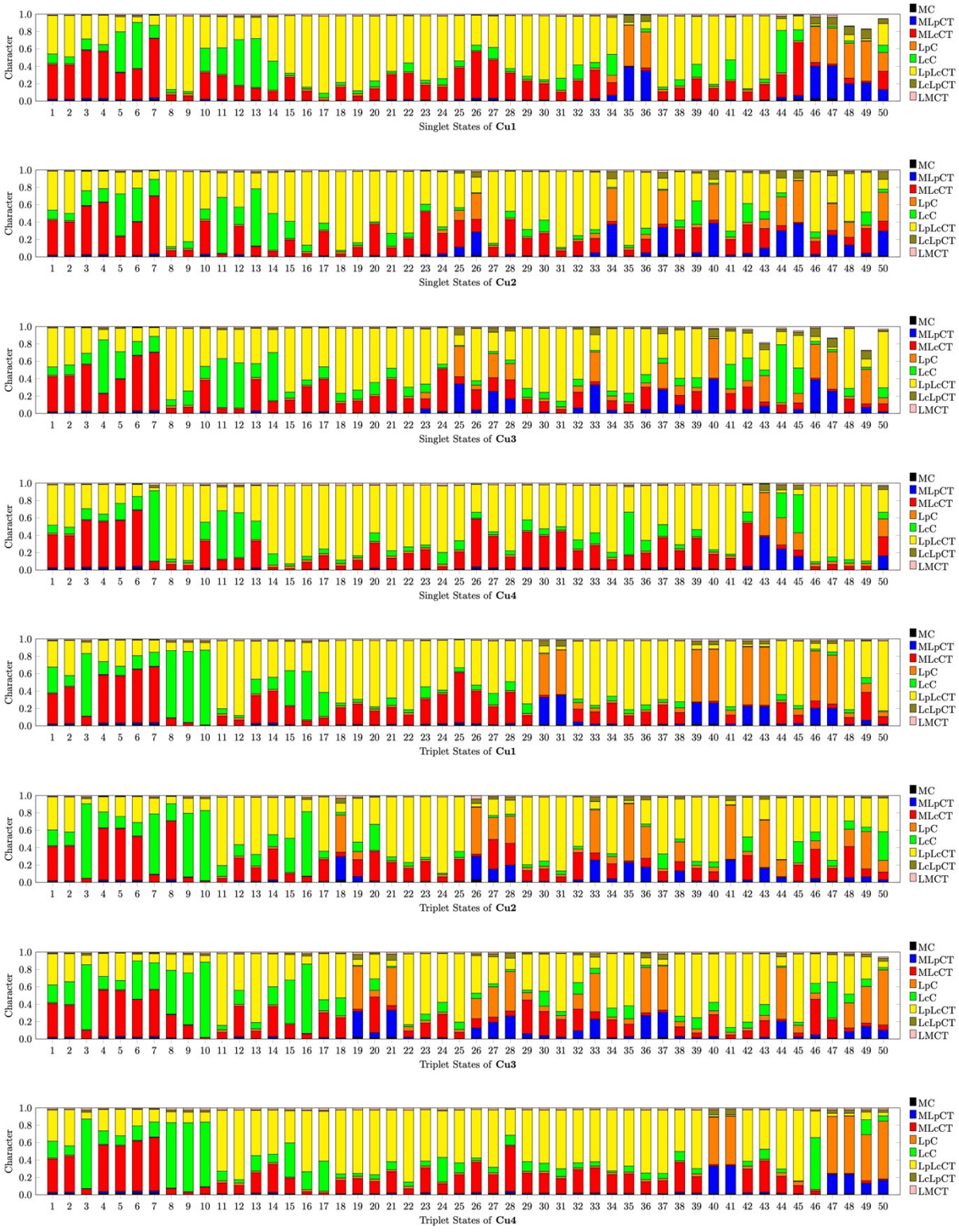

Figure S26. THEODore Analysis of the computed singlet (*top*) and triplet (*bottom*) states of the four complexes. L_P stands for the diphosphine ligand and L_C for the TzTz ligand.

LEC fabrication

LECs were fabricated on indium tin oxide (ITO)-coated glass substrates that were sequentially cleaned and treated with ultraviolet/ozone. A 40 nm layer of poly(3,4-ethylenedioxythiophene):poly(styrene sulfonate) (PEDOT:PSS) was deposited by spin coating at 3500 rpm and subsequently annealed at 150 °C for 30 min in air. The emissive layer was formed by spin coating a dichloromethane solution containing the copper complex (**Cu1** or **Cu4**) blended with the ionic liquid 1-butyl-3-methylimidazolium hexafluorophosphate [$BMIMPF_6$] (80:20 wt.%). The ionic liquid provided mobile ions to facilitate device operation. For **Cu4**-based devices, the emissive-layer thickness was controlled by varying the solution concentration from 50 to 70 mg mL^{-1} while spin coating at 2000 rpm for 60 s. For **Cu1**, owing to its limited solubility, a fixed concentration of 30 mg mL^{-1} was used and the film thickness was tuned by adjusting the spin-coating speed from 750 to 2000 rpm. Film thicknesses were measured by ellipsometry. After deposition, the devices were dried in a vacuum oven at 60 °C for 8 h to remove residual solvent. A silver top electrode was then thermally evaporated under a vacuum of $\approx 10^{-6}$ torr. Electroluminescence (EL) characteristics were measured using a source-measure unit (B2901A, Keysight) and a calibrated silicon photodiode, while EL spectra were recorded with a calibrated fiber-optic spectrometer (USB2000, Ocean Optics). All measurements were performed under constant voltage bias in a nitrogen-filled glovebox.

EL characteristics of LEC devices

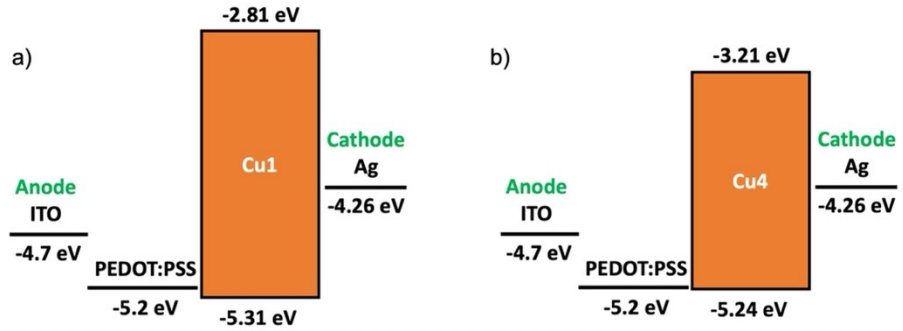

Figure S27. Energy level diagram of the materials employed for the fabrication of LEC devices comprising complex **Cu1** and **Cu4**.

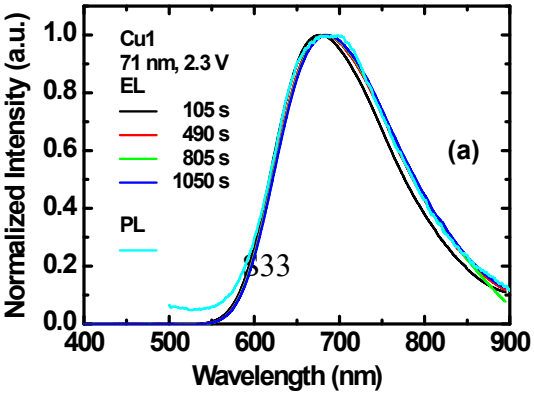

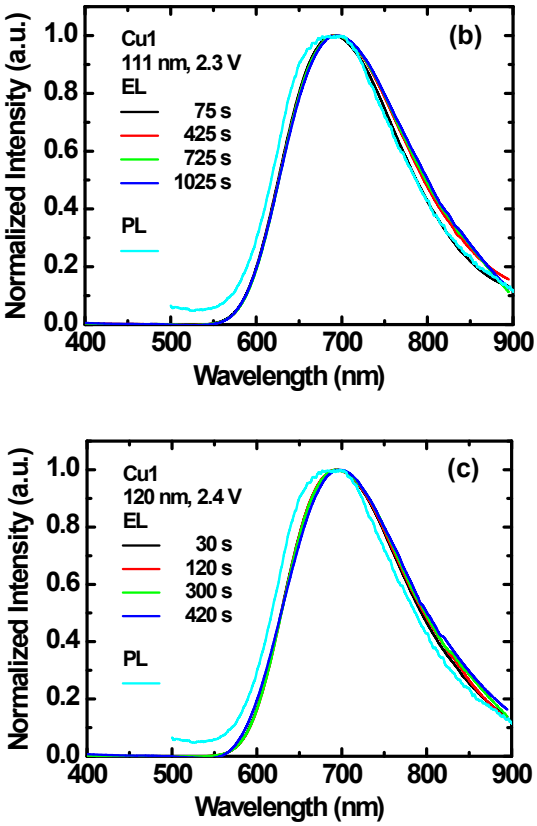

Figure S28. Time-dependent EL spectra of LECs based on complex **Cu1** with emissive layer thicknesses of (a) 71, (b) 111, and (c) 120 nm. The applied bias voltage is indicated in each panel. The PL spectrum of the emissive layer is shown for comparison.

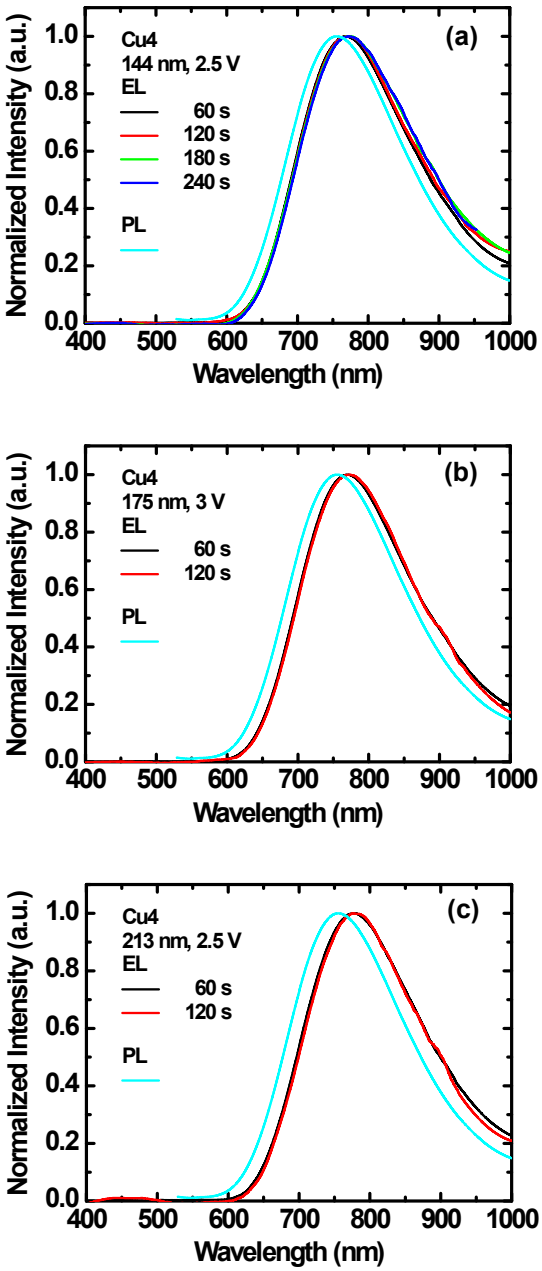

Figure S29. Time-dependent EL spectra of LECs based on complex **Cu4** with emissive layer thicknesses of (a) 144, (b) 175, and (c) 213 nm. The applied bias voltage is indicated in each panel. The PL spectrum of the emissive layer is shown for comparison.

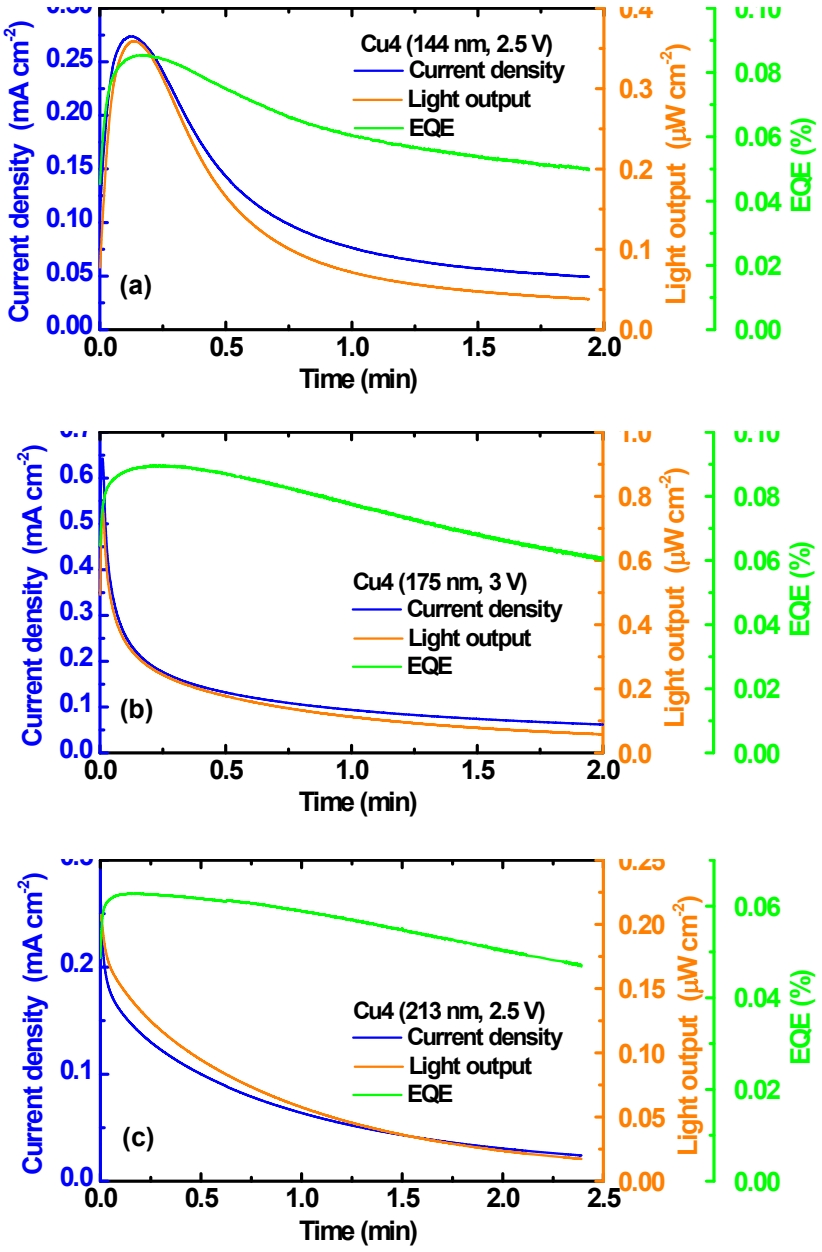

Figure S30. Time-dependent current density, light output, and EQE of LECs based on **Cu4** with emissive-layer thicknesses of (a) 144, (b) 175, and (c) 213 nm. The applied bias voltage is indicated in each panel.

References

1 M. Patanapongpibul, C. Zhang, G. Chen, S. Guo, Q. Zhang, S. Zheng, G. Wang and Q.-H. Chen, *Bioorg. Med. Chem.*, 2018, **26**, 4751–4760.
2 Bruker Corporation, *M86-EXX278V1 APEX4 User Manual*, 2021.
3 G. M. Sheldrick, *Acta Cryst. A Found Adv*, 2015, **71**, 3–8.
4 G. M. Sheldrick, *Acta Cryst. C*, 2015, **71**, 3–8.
5 A. L. Spek, *J. Appl. Cryst.*, 2003, **36**, 7–13.
6 G. A. Crosby and J. N. Demas, *J. Am. Chem. Soc.*, 1970, **92**, 7262–7270.
7 H. Ishida, S. Tobita, Y. Hasegawa, R. Katoh and K. Nozaki, *Coord. Chem. Rev.*, 2010, **254**, 2449–2458.
8 J. R. Lakowicz, *Principles of fluorescence spectroscopy*, Springer, New York, NY, Third edition, corrected at 4. printing., 2010.
9 S. Antonello, M. Musumeci, D. D. M. Wayner and F. Maran, *J. Am. Chem. Soc.*, 1997, **119**, 9541–9549.
10 A. Belèn Meneses, S. Antonello, M. C. Arévalo and F. Maran, *Electroanalysis*, 2006, **18**, 363–370.
11 A. J. Bard, L. R. Faulkner and H. S. White, *Electrochemical methods: fundamentals and applications*, Wiley, Hoboken, NJ, USA Chichester, West Sussex, UK, Third edition., 2022.
12 E. J. Baerends, N. F. Aguirre, N. D. Austin, J. Autschbach, F. M. Bickelhaupt, R. Bulo, C. Cappelli, A. C. T. van Duin, F. Egidi, C. Fonseca Guerra, A. Förster, M. Franchini, T. P. M. Goumans, T. Heine, M. Hellström, C. R. Jacob, L. Jensen, M. Krykunov, E. van Lenthe, A. Michalak, M. M. Mitoraj, J. Neugebauer, V. P. Nicu, P. Philipsen, H. Ramanantoanina, R. Rüger, G. Schreckenbach, M. Stener, M. Swart, J. M. Thijssen, T. Trnka, L. Visscher, A. Yakovlev and S. van Gisbergen, *J. Chem. Phys.*, 2025, **162**, 162501.
13 Vrije Universiteit, Amsterdam, ADF Manual 2025.1, http://www.scm.com, (accessed September 26, 2025).
14 P. J. Stephens, F. J. Devlin, C. F. Chabalowski and M. J. Frisch, *J. Phys. Chem.*, 1994, **98**, 11623–11627.
15 E. Van Lenthe and E. J. Baerends, *J. Comput. Chem.*, 2003, **24**, 1142–1156.
16 E. van Lenthe, A. Ehlers and E.-J. Baerends, *J. Chem. Phys.*, 1999, **110**, 8943–8953.
17 A. Klamt and G. Schüürmann, *J. Chem. Soc., Perkin Trans. 2*, 1993, 799–805.
18 S. Grimme, J. Antony, S. Ehrlich and H. Krieg, *J. Chem. Phys.*, 2010, **132**, 154104.
19 S. Hirata and M. Head-Gordon, *Chem. Phys. Lett.*, 1999, **314**, 291–299.
20 F. Plasser, *J. Chem. Phys.*, 2020, **152**, 084108.
21 E. F. Pettersen, T. D. Goddard, C. C. Huang, G. S. Couch, D. M. Greenblatt, E. C. Meng and T. E. Ferrin, *J. Comput. Chem.*, 2004, **25**, 1605–1612.
22 M. J. Frisch, G. W. Trucks, H. B. Schlegel, G. E. Scuseria, M. A. Robb, J. R. Cheeseman, G. Scalmani, V. Barone, G. A. Petersson, H. Nakatsuji, X. Li, M. Caricato, A. V. Marenich, J. Bloino, B. G. Janesko, R. Gomperts, B. Mennucci, H. P. Hratchian, J. V. Ortiz, A. F. Izmaylov, J. L. Sonnenberg, D. Williams-Young, F. Ding, F. Lipparini, F. Egidi, J. Goings, B. Peng, A. Petrone, T. Henderson, D. Ranasinghe, V. G. Zakrzewski, J. Gao, N. Rega, G. Zheng, W. Liang, M. Hada, M. Ehara, K. Toyota, R. Fukuda, J. Hasegawa, M. Ishida, T. Nakajima, Y. Honda, O. Kitao, H. Nakai, T. Vreven, K. Throssell, J. A. Montgomery, Jr., J. E. Peralta, F. Ogliaro, M. J. Bearpark, J. J. Heyd, E. N. Brothers, K. N. Kudin, V. N. Staroverov, T. A. Keith, R. Kobayashi, J. Normand, K. Raghavachari, A. P. Rendell, J. C. Burant, S. S. Iyengar, J. Tomasi, M. Cossi, J. M.

Millam, M. Klene, C. Adamo, R. Cammi, J. W. Ochterski, R. L. Martin, K. Morokuma, O. Farkas, J. B. Foresman, and D. J. Fox, *Gaussian 16*, Gaussian Inc., Wallingford CT, 2016.
23 A. D. Becke, *J. Chem. Phys.*, 1993, **98**, 5648–5652.
24 R. Ditchfield, W. J. Hehre and J. A. Pople, *J. Chem. Physi.*, 1971, **54**, 724–728.
25 S. Miertuš, E. Scrocco and J. Tomasi, *Chem. Phys.*, 1981, **55**, 117–129.
26 J. Contreras-García, E. R. Johnson, S. Keinan, R. Chaudret, J.-P. Piquemal, D. N. Beratan and W. Yang, *J. Chem. Theory Comput.*, 2011, **7**, 625–632.